ARTICLE

Bhlhe40 function in activated B and T_{FH} cells restrains the GC reaction and prevents lymphomagenesis

René Rauschmeier[1]*　, Annika Reinhardt[2,3]*　, Charlotte Gustafsson[4]　, Vassilis Glaros[2,3]　, Artem V. Artemov[5,6]　, Josefine Dunst[2,3]　, Reshma Taneja[7]　, Igor Adameyko[5,8]　, Robert Månsson[4,9]　, Meinrad Busslinger[1]　, and Taras Kreslavsky[2,3]　

The generation of high-affinity antibodies against pathogens and vaccines requires the germinal center (GC) reaction, which relies on a complex interplay between specialized effector B and CD4 T lymphocytes, the GC B cells and T follicular helper (T_{FH}) cells. Intriguingly, several positive key regulators of the GC reaction are common for both cell types. Here, we report that the transcription factor Bhlhe40 is a crucial cell-intrinsic negative regulator affecting both the B and T cell sides of the GC reaction. In activated CD4 T cells, Bhlhe40 was required to restrain proliferation, thus limiting the number of T_{FH} cells. In B cells, Bhlhe40 executed its function in the first days after immunization by selectively restricting the generation of the earliest GC B cells but not of early memory B cells or plasmablasts. Bhlhe40-deficient mice with progressing age succumbed to a B cell lymphoma characterized by the accumulation of monoclonal GC B-like cells and polyclonal T_{FH} cells in various tissues.

Introduction

Generation of high-affinity antibodies in response to pathogens and vaccines depends on a complex interplay between specialized subsets of activated antigen-specific B and T lymphocytes—germinal center (GC) B cells and T follicular helper (T_{FH}) cells—that takes place in the course of the GC reaction. Upon activation by cognate antigen, B cells undergo a burst of proliferation and differentiate into plasmablasts (PBs), non–GC-derived memory B cells (MBCs), or GC B cells (Glaros et al., 2021; Taylor et al., 2012a). The latter cells populate GCs, which are temporary microanatomic structures that form around follicular dendritic cell (FDC) clusters in B cell follicles of secondary lymphoid organs. The GC reaction is an iterative process that involves repetitive cycles of B cell proliferation, hypermutation of their antibody genes by activation-induced cytidine deaminase (AID), competition of the mutated B cell clones for antigen, and subsequent presentation of the processed antigen to a specialized T helper cell subset, T_{FH} cells (reviewed in Biram and Shulman, 2020; Crotty, 2019; De Silva and Klein, 2015; Mesin et al., 2016). T cell help provided by T_{FH} cells in

response to this antigen presentation is crucial for the survival and expansion of the B cell clones with higher BCR affinity. B cells eventually egress from the GC reaction to give rise to MBCs and high-affinity plasma cells (PCs). GCs can be divided histologically into a light zone (LZ), where B cells interact with FDCs, which capture and display antigen, and T_{FH} cells, and a dark zone (DZ), where proliferation and hypermutation take place. The GC reaction therefore involves continuous recirculation of B cells between the LZ and the DZ. A wave of expression of the transcription factor Myc that is transiently induced in the LZ proportionally to the magnitude of T cell help (Finkin et al., 2019) drives proliferation of GC B cells in the DZ (Calado et al., 2012; Dominguez-Sola et al., 2012), in part through induction of the Myc target gene *Tfap4* encoding the transcription factor AP4 (Chou et al., 2016). While the GC response is absolutely required for the generation of high-affinity antibodies, active mutagenesis in highly proliferative cells comes at a price, as dysregulation of the GC reaction can lead to lymphomagenesis. Indeed, a wide variety of B cell lymphomas,

[1]Research Institute of Molecular Pathology, Vienna Biocenter, Vienna, Austria;　[2]Department of Medicine, Division of Immunology and Allergy, Karolinska Institutet, Karolinska University Hospital, Stockholm, Sweden;　[3]Center for Molecular Medicine, Karolinska Institutet, Stockholm, Sweden;　[4]Center for Hematology and Regenerative Medicine, Department of Laboratory Medicine, Karolinska Institutet, Stockholm, Sweden;　[5]Department of Neuroimmunology, Medical University of Vienna, Vienna, Austria;　[6]Endocrinology Research Centre, Moscow, Russian Federation;　[7]Department of Physiology, Healthy Longevity Translational Research Program, Yong Loo Lin School of Medicine, National University of Singapore, Singapore;　[8]Department of Physiology and Pharmacology, Karolinska Institutet, Stockholm, Sweden;　[9]Hematology Center, Karolinska University Hospital, Stockholm, Sweden.

*R. Rauschmeier and A. Reinhardt contributed equally to this paper;　Correspondence to Taras Kreslavsky: Taras.Kreslavskiy@ki.se;　Meinrad Busslinger: Meinrad.Busslinger@imp.ac.at.

including follicular lymphoma, GC B cell–like diffuse large B cell lymphoma, Burkitt's lymphoma, Hodgkin's lymphomas, and a number of rarer lymphoma types, all originate from the GC reaction (Basso and Dalla-Favera, 2015).

For reasons that are not well understood, many key regulators of the GC reaction have cell-intrinsic functions in both GC B cells and T_{FH} cells. For example, mice deficient for the transcription factor Bcl6 completely lack GC responses, as Bcl6 is required for the differentiation of both GC B cells and T_{FH} cells (Dent et al., 1997; Fukuda et al., 1997; Nurieva et al., 2009; Ye et al., 1997; Yu et al., 2009). Although the molecular programs regulated by Bcl6 in GC B cells and T_{FH} cells are very different (Hatzi et al., 2015), Bcl6 functions in both cell types in part through the direct repression of Prdm1 that codes for the transcription factor Blimp1 (Shaffer et al., 2000). Blimp1 interferes with the GC B cell molecular program by promoting PC differentiation and shifting the balance of T helper cell differentiation from T_{FH} to T helper 1 (Johnston et al., 2009; Oestreich et al., 2012; Turner et al., 1994). The transcription factor Irf4 also promotes PC differentiation when expressed at high levels, while moderate amounts of Irf4 are required for the up-regulation of Bcl6 during the early phases of the GC response (Ochiai et al., 2013; Willis et al., 2014) as well as for T_{FH} cell differentiation (Bollig et al., 2012). GC formation is completely abrogated in the absence of the transcription factor Batf (Betz et al., 2010), which regulates expression of Bcl6 and Maf (Ise et al., 2011) in T_{FH} cells and is required for Ig class-switch recombination and cell expansion in GC B cells (Inoue et al., 2017; Ise et al., 2011). The transcription factor Foxo1 regulates DZ specification in GC B cells (Dominguez-Sola et al., 2015; Sander et al., 2015) and is required for late-stage GC T_{FH} cell differentiation, while inhibiting earlier steps of T_{FH} cell development (Stone et al., 2015). The list of such common regulators is not restricted to transcription factors, as mutations in Rc3h1 encoding the RNA-binding protein Roquin result in cell-intrinsic expansion of both GC B cells and T_{FH} cells (Bertossi et al., 2011; Vinuesa et al., 2005). Thus, a number of regulators, many of which are rapidly induced upon lymphocyte activation and therefore are likely to be part of the early response to antigen receptor signaling, play cell-intrinsic roles in both GC B cells and T_{FH} cells to orchestrate the GC response. Interestingly, while the action of these factors in GC B cells and T_{FH} cells is usually concordant in terms of overall positive effects on the GC response, the exact molecular and cellular functions of these common regulators are often very different in the two cell types.

While a number of transcription factors that positively regulate the GC reaction have been identified to date, relatively little is known about negative regulation of this process. It was previously reported that mice with germline deficiency of the transcription factor Bhlhe40 developed lymphoproliferation and mild autoimmunity with age (Sun et al., 2001). The disease was associated with enlarged GCs, but the mechanism causing this phenotype was not investigated. A later report demonstrated that aged Bhlhe40$^{-/-}$ mice exhibit decreased regulatory T cell numbers (Miyazaki et al., 2010), suggesting one possible explanation for this GC phenotype. In the present study, we aimed to test if Bhlhe40 could function as a cell-intrinsic negative

regulator in cells directly participating in the GC reaction. Unexpectedly, this analysis revealed that Bhlhe40 regulates both the T_{FH} and GC B cell arms of the GC response in a cell type–specific manner. In B cells, Bhlhe40 restrained the generation of the earliest GC B cells, but not early MBCs or PBs. In activated CD4 T cells, Bhlhe40 restrained proliferation throughout the response, thus limiting T_{FH} cell numbers. With age, the GC phenotype of Bhlhe40$^{-/-}$ mice culminated in the development of GC B cell lymphoma.

Results

A B cell–intrinsic function of Bhlhe40 in restraining the GC reaction

As our preliminary experiments (see below) demonstrated that Bhlhe40 is rapidly up-regulated upon in vitro B cell activation, we first aimed to test whether Bhlhe40 has a function in activated B cells. Analysis of Bhlhe40$^{-/-}$ mice revealed an increased number and size of spontaneous GCs in Bhlhe40 knockout (KO) mice (Figs. 1 A and S1 A) and demonstrated the accumulation of cells with GC B and T_{FH} cell phenotypes (Fig. 1, B and C; and Fig. S1 B). To test if this phenotype was caused by a cell-autonomous function of Bhlhe40 in B cells, we established and analyzed WT: Bhlhe40$^{-/-}$ mixed bone marrow (BM) chimeras. The overall frequencies of B and T cells originating from each donor closely reflected those observed in BM progenitors (Fig. S1 C), indicating that Bhlhe40 deficiency does not have a measurable impact on the overall development of T and B lymphocytes. However, the GC B cell compartment in spleens, lymph nodes, and Peyer's patches of these chimeras was dominated by cells originating from the KO donor (Figs. 1 D and S1 D). This phenotype was independent of the congenic marker used to identify KO cells (Figs. 1 D and S1 E), indicating that Bhlhe40 deficiency and not allelic variants of genes linked to Ptprc (CD45) are responsible for the phenotype. No further increase in GC B cell accumulation was observed when BM from mice double-deficient for Bhlhe40 and its close homologue Bhlhe41 was used to generate mixed BM chimeras, and no GC B cell phenotype was evident when Bhlhe41$^{-/-}$ BM was used (Fig. S1 F), indicating that Bhlhe40, but not Bhlhe41, negatively regulates the GC reaction. As the antigen specificity of "spontaneous" GC B cells observed in mixed BM chimeras is unclear, it was conceivable that their accumulation could have solely reflected some developmental defect (for example in tolerance formation) rather than a function of Bhlhe40 in B cell activation. The increase in KO GC B cells in Peyer's patches (Fig. 1 D) suggested that Bhlhe40 may restrain B cell responses to microbiota-derived antigens. To formally test if this transcription factor plays a role in the regulation of responses to foreign antigens, we next immunized mixed BM chimeras with PE. PE-specific GC B cells were likewise generated preferentially from KO donor B cells (Fig. 1 E). KO GC B cells exhibited a normal cell surface phenotype (Fig. 1, D and E), and the level of Ig class switching was indistinguishable from that of their WT counterparts (Fig. S1 G). The increased abundance of GC B cells in Bhlhe40$^{-/-}$ mice, however, was not directly translated into an increase in PCs, as judged by comparable numbers of antigen-specific antibody-secreting cells (ASCs) in the BM of WT and KO
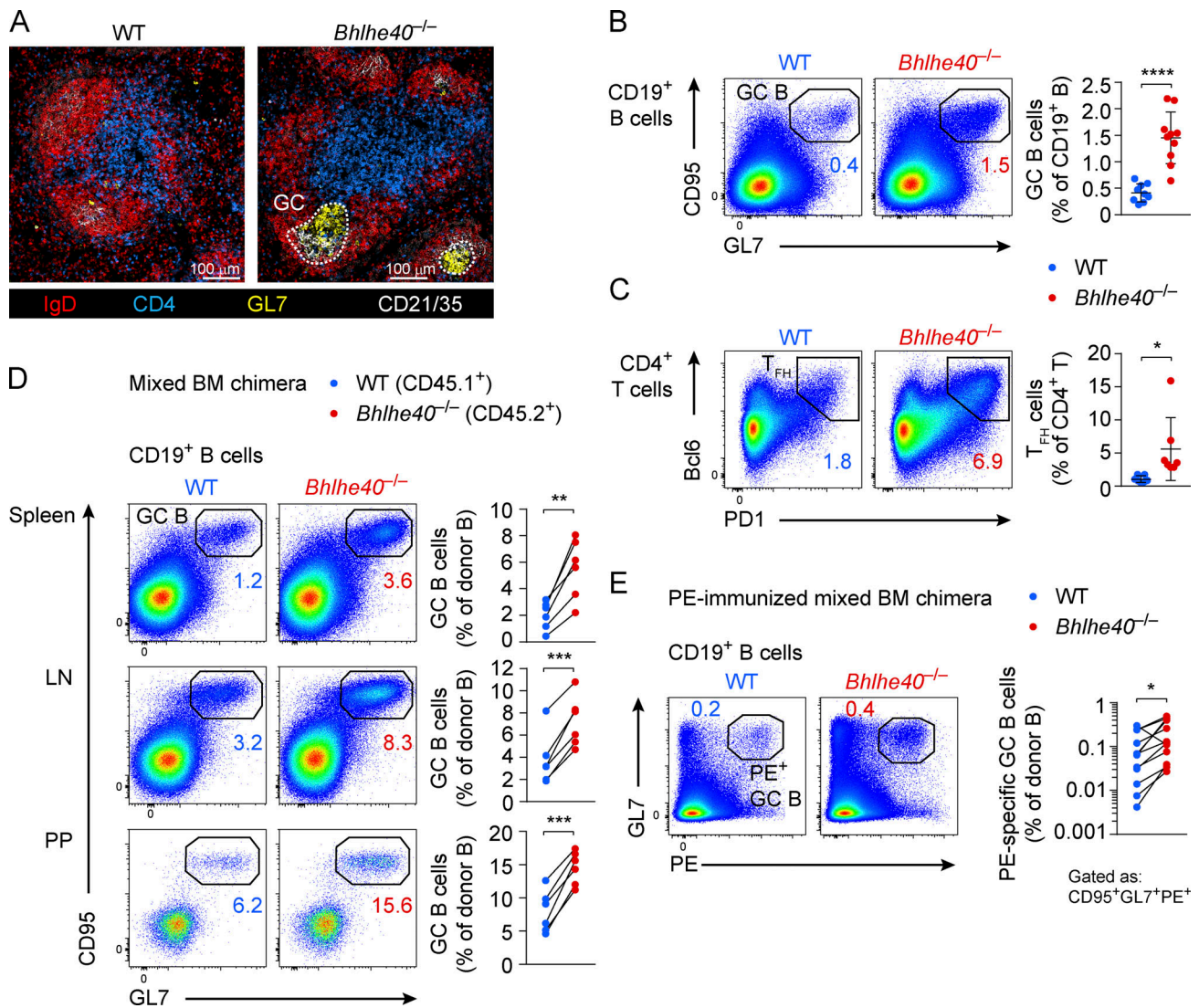
Rauschmeier et al.
Bhlhe40 in the germinal center reaction

Journal of Experimental Medicine   2 of 21
https://doi.org/10.1084/jem.20211406

Figure 1. **B cell–intrinsic function of Bhlhe40 restrains the GC reaction. (A)** Representative images of spleen sections of unchallenged WT and *Bhlhe40*^{−/−} mice as analyzed by confocal immunofluorescence microscopy. GCs were identified by GL7 (yellow) and CD21/CD35 (white) expression in IgD (red)-negative areas of B cell follicles. One of two independent experiments is shown. **(B and C)** Quantification of flow cytometric analysis of GC B cells (B) and T$_{FH}$ cells (C) in the spleens of unchallenged WT and *Bhlhe40*^{−/−} mice. Pooled data from two independent experiments with $n = 9$ (WT) and $n = 10$ (KO) mice (B) and $n = 7$ mice for each genotype (C) are shown. Surface expression of CD95 and GL7 on CD19^{+} B cells (B) and surface expression of PD1 and intracellular Bcl6 in CD4^{+} T cells (C) are shown. **(D and E)** Mixed BM chimeras were generated by transferring a 1:1 mixture of WT (CD45.1^{+}) and *Bhlhe40*^{−/−} (CD45.2[+]) BM progenitor cells into lethally irradiated *Rag2*^{−/−} recipients. Mice were analyzed >6 wk after transfer. **(D)** Flow cytometric analysis and quantification of the GC B cell population in spleen, peripheral LNs, and Peyer's patches (PP) in unchallenged mixed BM chimeras. One experiment with $n = 6$ mice is shown, representative of at least three independent experiments. **(E)** Mixed BM chimeras were immunized with PE emulsified in complete Freund's adjuvant. Antigen (PE)-specific GC B cells were analyzed by flow cytometry 21 d after immunization. GL7 expression and PE-binding on CD19^{+} B cells (left) and the quantification of PE-specific GC B cells (gated as CD95^{+}GL7^{+}PE^{+}) among donor CD19^{+} B cells (right) are shown. Pooled data from three independent experiments with $n = 12$ mice are shown. Data were analyzed with unpaired two-tailed Student's t test (in B and C, mean ± SD is shown) and paired two-tailed Student's t test (D and E). *, $P < 0.05$; **, $P < 0.01$; ***, $P < 0.001$; ****, $P < 0.0001$. One dot represents one mouse.

animals immunized with hapten 4-hydroxy-3-nitrophenylacetyl (NP) conjugated to OVA (Fig. S1 H). We therefore conclude that Bhlhe40 restrains the GC reaction at least in part through its functions in activated B cells.

Rapid transient up-regulation of *Bhlhe40* in activated B cells
As a first step to unravel at which time point of B cell activation Bhlhe40 could execute its function, we characterized the dynamics of its expression in activated B cells. In vitro, *Bhlhe40*

expression was rapidly and transiently induced to a maximal level ~1 h after stimulation with either anti-IgM or anti-CD40 antibodies, with CD40 cross-linking resulting in the highest expression (Fig. S2 A). These data suggest that both the exposure to antigen and interaction with T$_{FH}$ cells could be responsible for *Bhlhe40* induction in vivo. In line with this early up-regulation in activated B cells, published single-cell RNA-sequencing (scRNA-seq) analysis of human tonsillar B cells revealed highest *BHLHE40* expression in pre-GC B cells, a population suggested to

Rauschmeier et al.
Bhlhe40 in the germinal center reaction

Journal of Experimental Medicine 3 of 21
https://doi.org/10.1084/jem.20211406

represent immediate GC B cell precursors in this dataset (Fig. S2 B; King et al., 2021). Analysis of mouse datasets from the Imm-Gen database (Yoshida et al., 2019) revealed overall low *Bhlhe40* expression in GC B cells, with a higher level of expression in the LZ than in the DZ GC B cells (Fig. S2 C). As several other important regulators of the GC reaction, including Myc and AP4, are also expressed lowly in bulk GC B cells, but are thought to be transiently induced to high levels in a small subset of LZ GC B cells upon interaction with T$_{FH}$ cells and/or antigen (Calado et al., 2012; Chou et al., 2016; Dominguez-Sola et al., 2012), we next assessed *Bhlhe40* expression at the single-cell level by RNA flow cytometry. Indeed, *Bhlhe40* was expressed by a subset of LZ GC B cells (Fig. S2 D). Bhlhe40 deficiency, however, did not affect the ratio between LZ and DZ GC B cells (Fig. S2 E). We conclude that *Bhlhe40* is rapidly but transiently induced upon B cell activation and that its expression in a subset of LZ GC B cells may likewise reflect transient induction upon interaction with antigen and/or T$_{FH}$ cells.

Bhlhe40 restricts the generation of the earliest GC B cells

The expression analysis described above suggested that Bhlhe40 could execute its function early upon B cell activation after the initial interaction with antigen and/or T$_{FH}$ cells, as well as later in the response, during the course of the ongoing GC reaction, through its transient induction in the LZ. To start addressing these possibilities, we aimed to test at which point of the response the Bhlhe40-deficient B cells gain their competitive advantage. To have sufficient cell numbers for characterization of the earliest stages of the response, we crossed *Bhlhe40$^{-/-}$* mice to B1-8^{hi} *Igh* knock-in mice, in which B cells with λ light chains (Igλ) recognize NP (Shih et al., 2002). We then cotransferred congenically distinguishable *Bhlhe40$^{-/-}$Igh$^{B1-8hi/+}$* and *Bhlhe40$^{+/+}$Igh$^{B1-8hi/+}$* splenocytes (with confirmed 1:1 ratio of Igλ$^+$ B cells) into WT recipients, followed by NP-OVA immunization (Fig. 2 A). In line with observations made for the polyclonal responses to PE (Fig. 1 E), these experiments demonstrated that the majority of donor-derived GC B cells were originating from the KO donor (Fig. 2, B and C). The competitive advantage of Bhlhe40-deficient cells was evident for the first GC B cells that emerged around day 3 after immunization, reached its maximum by day 6 after immunization, and remained stable thereafter (Fig. 2 C). These results suggested that Bhlhe40 restrains the earliest stages of the GC reaction and that Bhlhe40 expression in B cells may become dispensable in mature GCs. We therefore focused our attention on the events that take place during the emergence of the first GC B cells around day 3–5 after immunization. At this point, activated Igλ$^+$ B1-8^{hi} B cells formed three distinct populations: CD138$^+$ early PBs, a CCR6$^+$GL7$^{lo/int}$ population likely including non–GC-derived early MBCs as well as common precursors for all activated cell populations (Glaros et al., 2021; Schwickert et al., 2011; Taylor et al., 2012a; Taylor et al., 2012b), and CCR6$^-$GL7^{hi} early GC B cells (Fig. 2 B). Strikingly, while in the competitive transfer experiments KO B1-8^{hi} B cells exhibited a clear advantage in the GC B cell compartment, ratios in both PBs and in the CCR6$^+$ activated B cell population closely reflected the ratio in Igλ$^+$ B cells at the time of the transfer (Fig. 2 B). Of note, no difference in the Bcl6 expression

level was observed for WT and KO GC B cells (Fig. S2 F). The phenotype was the same when congenic markers on WT and KO B1-8^{hi} B cells were inverted (Fig. S2 G). WT and KO GC B cells exhibited identical levels of Ig class switching (Fig. S2 H). Moreover, similar frequencies of IRF4$^+$ PC and CCR6$^+$ MBC precursors (Fig. S2, I and J; Ise et al., 2018; Suan et al., 2017) were detected in WT and KO LZ GC B cells, suggesting that Bhlhe40 deficiency does not affect GC output, at least at early stages of PC and MBC differentiation.

RNA flow cytometry experiments demonstrated that *Bhlhe40* was expressed by the majority of cells in the CCR6$^+$ cell population on day 4 after immunization and was subsequently downregulated in the early GC B cells (Fig. 2 D). These results suggest that Bhlhe40 functions in the CCR6$^+$ activated B cells and may limit their contribution to the GC B cell compartment. Of note, no competitive advantage of *Bhlhe40$^{-/-}$* B1-8^{hi} B cells was observed upon immunization with the T cell–independent antigen NP-Ficoll, even when gating for cells with a GC B-like phenotype, which are known to be generated in T-independent responses (Fig. 2 E; de Vinuesa et al., 2000; Shih et al., 2002), was applied. Taken together, these results demonstrated that Bhlhe40 is a highly selective negative regulator of the earliest GC B cells that restrains the immune responses to T cell–dependent antigens.

As Bhlhe40 is a negative regulator of proliferation in several cell types (Kreslavsky et al., 2017; Ow et al., 2014), we next tested if Bhlhe40 deficiency affects proliferation of GC B cells or the CCR6$^+$ activated B cell population. For this, we focused on the time point when the very first GC B cells were detectable in most of the mice. Incorporation of 5-ethynyl-2'-deoxyuridine (EdU) by B1-8^{hi} WT and KO B cells was comparable, and GC B cells of both genotypes exhibited much higher frequencies of EdU$^+$ cells than the CCR6$^+$ population (Fig. 3 A). Expectedly, no difference in EdU incorporation was detectable at later time points (data not shown) or in spontaneous GC B cells in mixed BM chimeras (Fig. S3 A). Proliferation of in vitro activated B cells was also comparable between cocultured WT and KO B cells across a range of anti-IgM and anti-CD40 concentrations, and the ratio between WT and KO B cells remained stable in these cultures (Fig. S3 B), suggesting that, at least in vitro, survival of B cells is also not affected by Bhlhe40 deficiency. Moreover, Bhlhe40 deficiency also did not result in any measurable change in the frequency of cleaved caspase-3–positive B1-8^{hi} B cells in vivo, and very little apoptosis took place in GC B cells at these early time points, irrespectively of their genotype (Fig. 3 B). Likewise, apoptosis of polyclonal GC B cells was not affected by Bhlhe40 deficiency in mature GCs in mixed BM chimeras (Fig. S3 C). Finally, the distribution of WT and KO Igλ$^+$B1-8^{hi} B cells was also indistinguishable outside of GCs on days 2 and 4 after immunization (Fig. S3 D), suggesting that Bhlhe40 deficiency does not grossly affect the localization of early activated B cells.

The results described above suggested that Bhlhe40 is unlikely to regulate the size of the GC B cell compartment through effects on apoptosis, proliferation, or migration. We therefore hypothesized that Bhlhe40 could act through limiting the differentiation of activated cells to the GC B cell "lineage." To find evidence for or against this hypothesis, we performed bulk
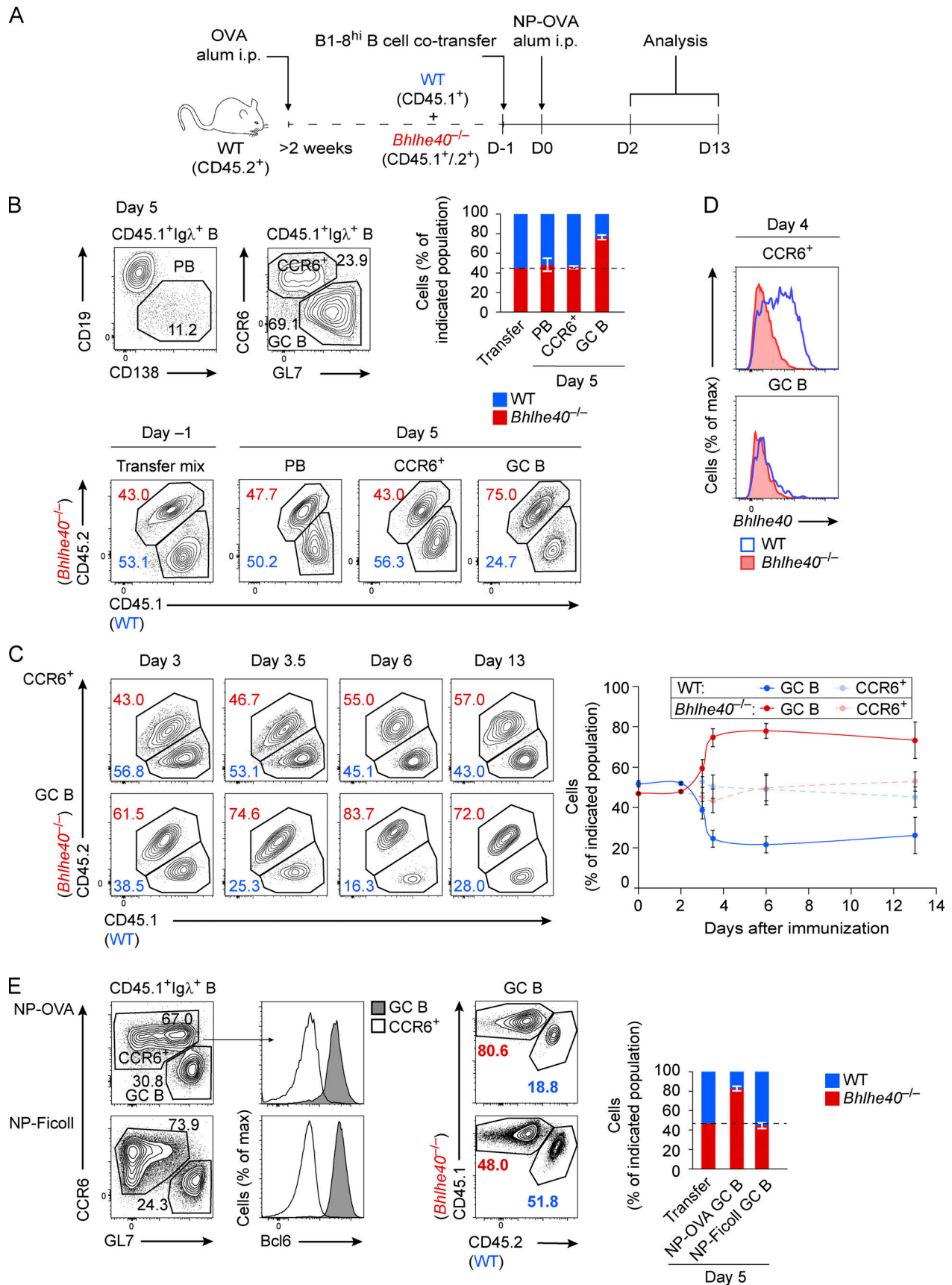
Rauschmeier et al.
Bhlhe40 in the germinal center reaction

Journal of Experimental Medicine 4 of 21
https://doi.org/10.1084/jem.20211406

Figure 2. **Bhlhe40 restricts the earliest stages of the GC B cell response. (A)** Schematic representation of the experimental setup for B and C. OVA-primed CD45.2[+] WT mice were injected with a 1:1 mixture of WT (CD45.1[+]) and *Bhlhe40*^{−/−} (CD45.1[+]/CD45.2^{+}) B1-8^{hi} splenocytes and immunized with NP-OVA in alum

the next day. **(B)** Top: Surface expression of CD138, CCR6, and GL7 on CD45.1⁺Igλ⁺CD19⁺ B cells (intracellular Igλ staining for PB gating) and quantification of WT and *Bhlhe40⁻/⁻* donor-derived cells among total CD45.1⁺Igλ⁺CD19⁺ B cells at the time of the transfer, as well as among PBs, CCR6⁺ cells, and GC B cells on day 5 after immunization. One experiment with $n = 4$ mice is shown, representative of three independent experiments. **(C)** Representative flow cytometric analysis and quantification of WT and *Bhlhe40⁻/⁻* donor-derived cells among CD45.1⁺Igλ⁺CD19⁺CCR6⁺ and GC B cells at the indicated time points after immunization. Gating for total Igλ⁺CD19⁺ B cells was applied for day 0 (transfer mix) and day 2 (before GC B cell emergence) after immunization. The time course is based on pooled data from two independent experiments with $n = 4$–16 mice for each time point. One dot represents the mean with SD for each time point. **(D)** Expression of *Bhlhe40* was assessed by RNA flow cytometry in NP-specific (Igλ⁺) B1-8ʰⁱ donor-derived GC B cells (CCR6⁻GL7⁺) and CCR6⁺ B cells on day 4 after NP-OVA immunization. The experiment was designed as in A, except for the use of CD45.1⁺/CD45.2⁺ WT and CD45.1⁺ *Bhlhe40⁻/⁻* B1-8ʰⁱ splenocytes. The results are representative of two independent experiments. **(E)** Surface expression of CCR6 and GL7 on CD45.1⁺Igλ⁺CD19⁺ B cells as well as intracellular expression of Bcl6 in CCR6⁺ and GL7⁺ CD45.1⁺Igλ⁺CD19⁺ B cells on day 5 after immunization with NP-OVA or NP-Ficoll in alum. OVA-primed and unprimed recipients were used for NP-OVA and NP-Ficoll groups, respectively. Quantification of WT and *Bhlhe40⁻/⁻* donor-derived cells among cells with a GC B cell phenotype is depicted. One experiment with $n = 5$ mice per condition is shown, representative of two independent experiments.

RNA-seq on double-sorted WT and KO CCR6⁺ and GC B cell populations from the B1-8ʰⁱ cotransfer system described above on day 4 after immunization. This analysis revealed very limited changes in gene expression between WT and KO cells, with less than a dozen genes significantly (adjusted P value <0.1, fold-change ≥2) changing their expression in the KO cells (Fig. S4 A). None of these genes coded for proteins that could be connected to the observed phenotype. In line with the results obtained with RNA flow cytometry (Fig. 2 D), *Bhlhe40* was expressed in CCR6⁺ cells but was almost completely downregulated in the early GC B cells (Fig. S4 B). These results suggest that *Bhlhe40* functions in precursors of early GC B cells within the CCR6⁺ activated B cell population. Indeed, gene set enrichment analysis (GSEA) demonstrated that a GC B cell signature gene set (Mabbott and Gray, 2014) was mildly but significantly up-regulated in KO CCR6⁺ B cells compared with their WT counterparts (Fig. 3 C). Likewise, GSEA using the top 500 genes that were expressed more highly in day 4 WT GC B cells than in WT CCR6⁺ activated B cells (early GC B cell signature) revealed up-regulation of this gene set in the KO CCR6⁺ population (Fig. 3 C). Overall, changes in gene expression were mild, and from the genes included in this signature only up-regulation of *Mgll* and *Igj* reached statistical significance (Fig. S4 A). To test if Bhlhe40 may directly repress some of these GC B cell signature genes, we performed chromatin immunoprecipitation coupled with deep sequencing (ChIP-seq) detection of the genome-wide Bhlhe40 binding in naive B cells stimulated in vitro for 4 h with anti-CD40 antibody. This analysis demonstrated enrichment of the expected CTCGTG E-box motif in Bhlhe40 peaks, revealed the preferential promoter and gene body binding of Bhlhe40 (Fig. S4 C), and suggested that some of the GC B cell signature genes up-regulated in the KO cells (Fig. 3 C) may indeed be directly repressed by Bhlhe40 (Fig. S4 D). Taken together, these results suggest that Bhlhe40 may act through a mild but broad repression of GC B cell signature genes in the CCR6⁺ activated B cell population.

We next compared WT and KO Igλ⁺B1-8ʰⁱ B cells from days 3.5 and 4 (time points pooled) after immunization by scRNA-seq. An additional WT dataset from day 2.5 after immunization was included in the initial analysis to better define the population structure of early B cell activation and to capture the developmental transitions. Comparison of WT and KO cells was then performed using cells from day 3.5–4 only. As described in detail elsewhere (Glaros et al., 2021), this analysis confirmed that

activated B cells on day 3.5–4 formed three distinct groups corresponding to GC B cells, PBs, and the CCR6⁺ population containing activated precursors and early MBCs (Fig. S4 E). In line with the results obtained by flow cytometry (Fig. 2 D) and bulk RNA-seq (Fig. S4 B), *Bhlhe40* expression was limited to the CCR6⁺ cell population in our scRNA-seq data (Fig. S4 F). Both WT and KO cells were present across all the populations, but as expected, KO cells were enriched among GC B cells (Fig. 3 D). Similar to the bulk RNA-seq results, scRNA-seq revealed only minor changes in gene expression between WT and KO populations (data not shown). To test if Bhlhe40 influences GC B cell differentiation, we next ranked cells by their level of expression of GC B cell signature genes (Fig. 3 D [right] and Fig. S4 G) and assessed the ratio between WT and KO cells along this trajectory. To this end, normalized read counts for GC B cell signature genes (Mabbott and Gray, 2014; see Materials and methods for further details) were summed for each cell to calculate the strength of GC B cell signature expression, cells were binned according to this value, and the frequency of WT and KO cells in each bin was quantified. This analysis revealed that up-regulation of the GC B cell signature coincided with a gradual increase in the relative frequency of KO cells (Fig. 3 D, right), indicating that Bhlhe40-deficient B cells gained a competitive advantage at the earliest steps of GC B cell differentiation and suggesting their possible accelerated progression along this differentiation trajectory. Taken together, these results suggest that Bhlhe40 restrains the generation of the earliest GC B cells, that Bhlhe40-deficient cells gain their competitive advantage gradually in the course of early GC B cell differentiation, and that Bhlhe40 may function by directly repressing genes of the GC B cell program genes in early activated B cells.

A T cell–intrinsic function of Bhlhe40 restrains the T_FH cell response

The results described above clearly identified a cell-intrinsic function of Bhlhe40 in activated B cells. To test if increased GC activity in *Bhlhe40⁻/⁻* mice can be fully explained by its role in B lymphocytes, we sought to inactivate *Bhlhe40* selectively in this cell type. To this end, we generated a new conditional allele of *Bhlhe40* (Fig. S5 A) and crossed mice carrying this allele to a panel of Cre lines. Ablation of *Bhlhe40* in all hematopoietic cells with *Vav1*-Cre phenocopied the steady-state GC B and T_FH cell phenotypes of *Bhlhe40⁻/⁻* mice, indicating that they can be fully explained by Bhlhe40 function in the hematopoietic system

Rauschmeier et al.
Bhlhe40 in the germinal center reaction

Journal of Experimental Medicine   6 of 21
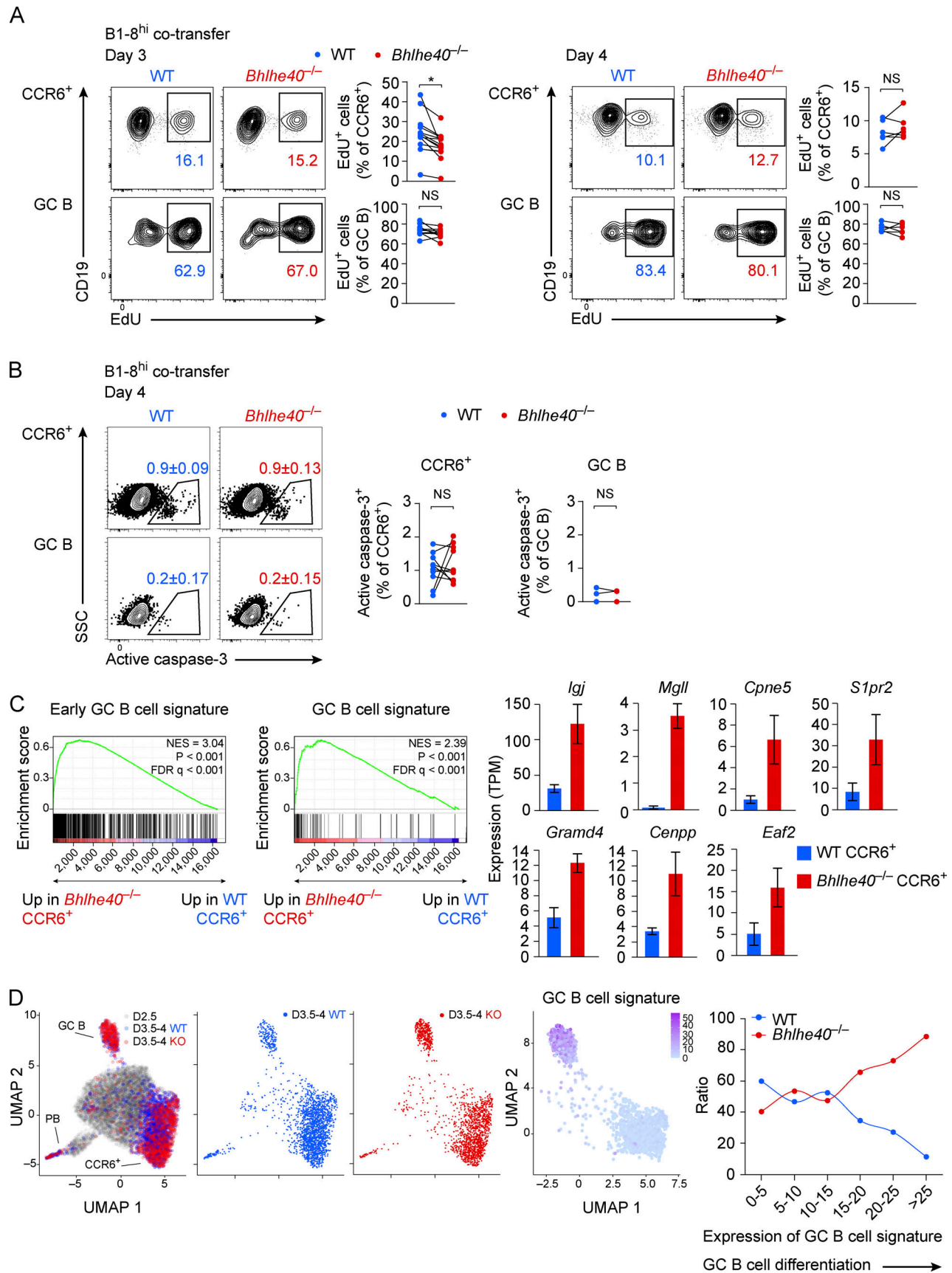https://doi.org/10.1084/jem.20211406

Figure 3. **Bhlhe40 restrains the generation of early GC B cells. (A–D)** OVA-primed CD45.2+ WT mice were injected with a 1:1 mixture of WT (CD45.1+) and *Bhlhe40*−/− (CD45.1+/CD45.2+; A [day 3], C, and D) or WT (CD45.1+/CD45.2+) and *Bhlhe40*−/− (CD45.1+; A [day 4] and B) B1-8hi splenocytes, followed by

Rauschmeier et al.
Bhlhe40 in the germinal center reaction

Journal of Experimental Medicine
https://doi.org/10.1084/jem.20211406

immunization with NP-OVA in alum next day. **(A and B)** Flow cytometric analysis and quantification assessing the proliferation (A) and frequency of apoptotic cells (B) of WT and *Bhlhe40*$^{-/-}$ CCR6$^+$ and GC B cells on day 3 (A) and 4 (A and B) after immunization. In A, EdU was i.v. injected 4 and 2 h before analysis. In B, apoptotic cells were identified by intracellular staining for active caspase-3. SSC, side scatter. One experiment with n = 14 (day 3) and n = 6 (day 4) mice is shown in A. Representative of at least two independent experiments. Pooled data from two independent experiments with n = 10 mice are shown in B. Note that active caspase-3$^+$ cells were detectable in the GC B cell compartment of only 2 of 10 mice analyzed. Flow cytometry plots show electronically merged data from three mice, and the mean values with SD are shown. Data were analyzed with paired two-tailed Student's t test; NS, P > 0.05; *, P < 0.05. One dot represents one mouse. **(C)** Left: RNA-seq data of WT and *Bhlhe40*$^{-/-}$ CCR6$^+$ B1-8^{hi} B cells on day 4 after immunization were used for GSEA with a published GC B cell signature (Mabbott and Gray, 2014; GC B cell signature) or the top 500 genes up-regulated in WT day 4 B1-8^{hi} GC B cells compared with WT day 4 CCR6$^+$ B cells (early GC B cell signature) as gene sets. Genes were ranked on the basis of fold expression changes in *Bhlhe40*$^{-/-}$ CCR6$^+$ B cells versus WT CCR6$^+$ B cells. FDR, false discovery rate; NES, normalized enrichment score. Right: The expression of selected genes that were enriched in *Bhlhe40*$^{-/-}$ CCR6$^+$ B1-8^{hi} B cells as identified by GSEA are shown in WT and *Bhlhe40*$^{-/-}$ CCR6$^+$ B cells as assessed by RNA-seq analysis on day 3.5–4 after immunization. TPM, transcripts per million. **(D)** scRNA-seq comparison of WT and KO GC B cell differentiation. Left: UMAP plots showing the distribution of WT (days 2.5 and/or 3.5–4 after immunization) and KO (days 3.5–4 after immunization) B1-8^{hi} B cells. Middle: UMAP plot showing the expression of GC B cell signature genes in clusters that were included for the subsequent WT/KO comparison. Right: The frequencies of WT (blue) and KO (red) B cells among cells binned according to the expression level of GC B cell signature genes.

(Fig. 4 A). Unexpectedly, while deletion of *Bhlhe40* in B cells with *Mb1*-Cre (active from the pro-B cell stage on) also resulted in a GC B and T$_{FH}$ cell increase, the phenotype was markedly less pronounced (Fig. 4 B) compared with *Vav1*-Cre *Bhlhe40*$^{fl/fl}$ and *Bhlhe40*$^{-/-}$ mice, despite the equally high deletion efficiencies observed with both Cre lines in B cells (Fig. S5 B). Inactivation of *Bhlhe40* with *Cd23*-Cre in immature B cells during later B cell development recapitulated the phenotype observed with *Mb1*-Cre–mediated deletion (Fig. 4 C), while no phenotype was observed in *Aicda*-Cre *Bhlhe40*$^{fl/fl}$ mice (Fig. 4 D). As *Aicda*-Cre is predominantly active in GC B cells that express the highest level of *Aicda* (encodes AID), these results are in line with the notion that Bhlhe40 functions in a narrow time window very early in GC B cell differentiation and that it is dispensable in mature GC B cells. The discrepancy in the magnitude of the phenotypes observed in B cell–specific (Fig. 4, B and C) and pan-hematopoietic (Fig. 4 A) *Bhlhe40* KOs indicated that inactivation of Bhlhe40 in another cell type in the hematopoietic system may contribute to the overall phenotype in *Bhlhe40*$^{-/-}$ and *Vav1*-Cre *Bhlhe40*$^{fl/fl}$ mice. In search for this additional cell type, we next deleted *Bhlhe40* in T cells with *Cd4*-Cre. Strikingly, this also resulted in a measurable increase of both the T$_{FH}$ cell and GC B cell compartments (Fig. 4 E). Thus, Bhlhe40 restrains the GC reaction through its cell-intrinsic functions both in B and T lymphocytes. Of note, the inactivation of *Bhlhe40* in B cells, in addition to an increase in GC B cells, resulted in accumulation of T$_{FH}$ cells (Fig. 4, B and C), and the ablation of *Bhlhe40* in T cells also positively affected both T$_{FH}$ cell and GC B cell numbers (Fig. 4 E). The strongest accumulation of GC B cells was observed when Bhlhe40 was absent in both cell types (Fig. 4 A). Thus, in addition to cell-intrinsic functions of Bhlhe40 in activated B cells and T$_{FH}$ cells, the GC phenotype is further amplified through a positive feedback loop likely mediated by interactions between these two cell types. These observations are in line with a previously reported strong direct correlation between numbers of GC B cells and T$_{FH}$ cells (Baumjohann et al., 2013).

As it was previously reported that aged *Bhlhe40*$^{-/-}$ mice have decreased numbers of regulatory T cells (Miyazaki et al., 2010), we next analyzed the Foxp3$^+$ T cell compartment of Bhlhe40-deficient mice. Indeed, *Bhlhe40*$^{-/-}$ and *Cd4*-Cre *Bhlhe40*$^{fl/fl}$ mice already at the age of 14–15 wk exhibited a mild decrease in the frequency of Foxp3$^+$ CD4 T cells (Fig. 4 F). Nevertheless, no

corresponding decrease in Bcl6$^+$PD1$^+$Foxp3$^+$ CD4 T follicular regulatory (T$_{FR}$) cells was observed, and if anything, their abundance was slightly increased in *Cd4*-Cre *Bhlhe40*$^{fl/fl}$ mice (Fig. 4 G). The overall increase in T$_{FH}$ cells, however, resulted in a strongly decreased T$_{FR}$/T$_{FH}$ cell ratio (Fig. 4 G), which possibly contributes to the increased GC reaction in the absence of Bhlhe40.

We next aimed to test if Bhlhe40 executes its function upon T cell activation. In line with this possibility, *Bhlhe40* was previously shown to be rapidly induced upon TCR cross-linking in naive T cells (Li et al., 2019; Miyazaki et al., 2010) and was expressed in T$_{FH}$ cells (Fig. 5 A). To further characterize the function of Bhlhe40 in CD4 T cells, we once again took advantage of the WT:*Bhlhe40*$^{-/-}$ mixed BM chimera approach. As for GC B cells, spontaneous T$_{FH}$ cells in mixed BM chimeras were preferentially generated from KO cells (Figs. 5 B and S5 C). A less pronounced increase was also observed in activated non-T$_{FH}$ CD4 T cells (Fig. 5 B). These results suggest that Bhlhe40 expression has a negative impact on the activated CD4 T cell compartment, and this impact is stronger in the case of the T$_{FH}$ cell subset. To test if this phenotype can be recapitulated in response to a foreign antigen, we next immunized mixed BM chimeras with the peptide antigens Ag85b$_{280-294}$ or 2W1S in complete Freund's adjuvant. Quantification of the responding cells from both donors with MHC class II tetramers revealed a significant increase in the frequency of antigen-specific CD4 T cells derived from the KO donor cells (Figs. 5 C and S5 D), and the vast majority of these cells had a PD1$^+$CXCR5$^+$ T$_{FH}$ cell phenotype (Fig. 5 C). We conclude that, in addition to its function in B cells, Bhlhe40 restrains the T$_{FH}$ cell response in a cell-intrinsic manner.

Bhlhe40 restrains T$_{FH}$ cell proliferation
As Bhlhe40 and its close homologue Bhlhe41 were reported to have moderate antiproliferative effects in a number of cell types (Ow et al., 2014), we next tested if the competitive advantage of Bhlhe40-deficient antigen-specific CD4 T cells in mixed BM chimeras was caused by their increased proliferation. Indeed, tetramer-positive KO CD4 T cells showed significantly increased EdU incorporation when compared with their WT counterparts (Fig. 5 D). RNA-seq comparison of WT and KO tetramer-positive cells revealed up-regulation of signatures associated with cell

Rauschmeier et al.
Bhlhe40 in the germinal center reaction

Journal of Experimental Medicine   8 of 21
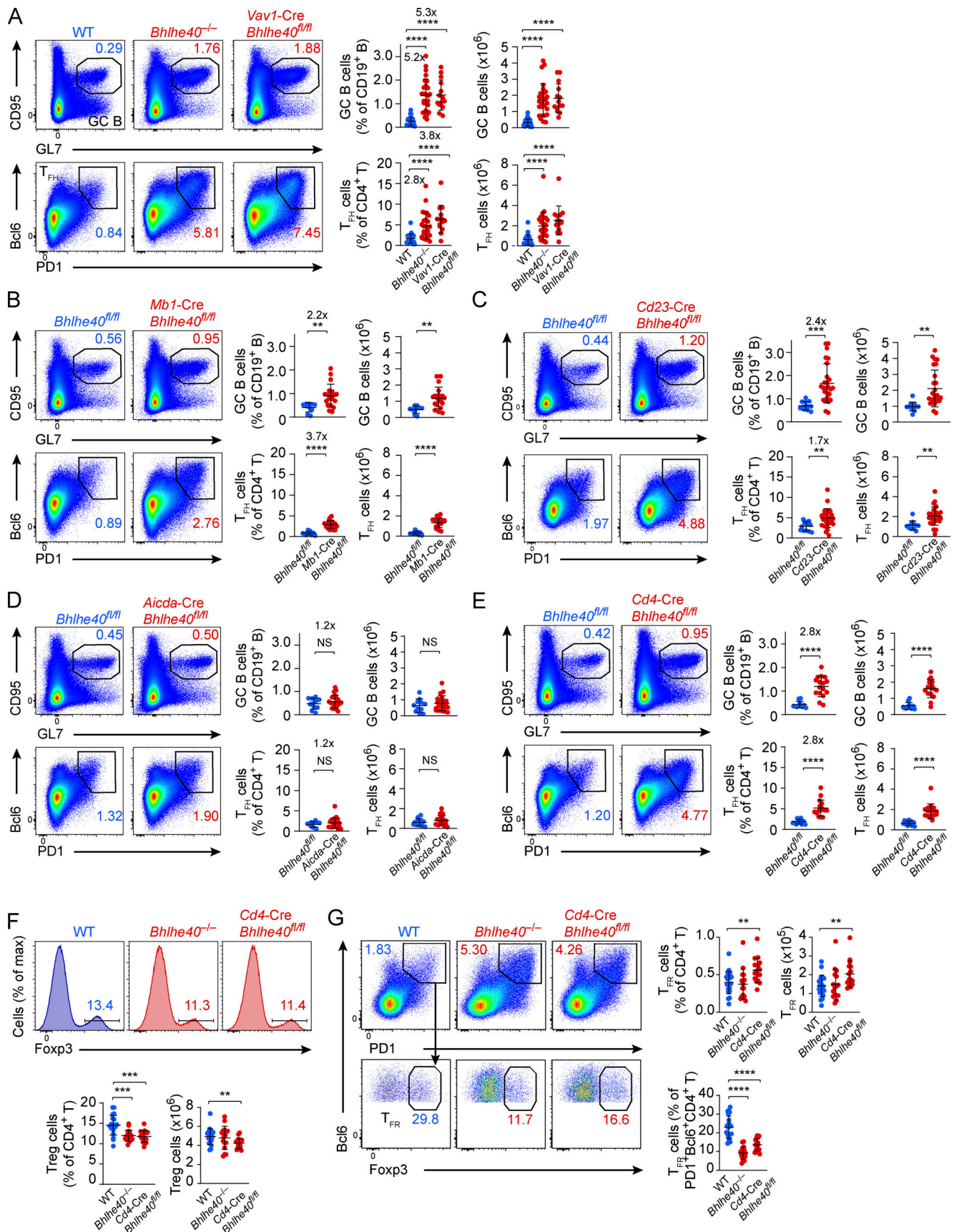https://doi.org/10.1084/jem.20211406

Figure 4. **Bhlhe40 restrains the GC reaction through its cell-intrinsic functions in both B and T cells. (A–E)** Flow cytometric analysis and quantification of GC B cells and T_{FH} cells in unchallenged WT, *Bhlhe40*$^{-/-}$, and *Vav1*-Cre *Bhlhe40*$^{fl/fl}$ mice (A); *Bhlhe40*$^{fl/fl}$ and *Mb1*-Cre *Bhlhe40*$^{fl/fl}$ mice (B); *Bhlhe40*$^{fl/fl}$ and *Cd23*-

Cre *Bhlhe40*^fl/fl mice (C); *Bhlhe40*^fl/fl and *Aicda*-Cre *Bhlhe40*^fl/fl mice (D); and *Bhlhe40*^fl/fl and *Cd4*-Cre *Bhlhe40*^fl/fl mice (E). Pooled data from three independent experiments with n = 24 (WT), n = 27 (*Bhlhe40*^−/−), n = 14 (*Vav1*-Cre *Bhlhe40*^fl/fl; A); n = 10 (*Bhlhe40*^fl/fl) and n = 19 (*Mb1*-Cre *Bhlhe40*^fl/fl; B); n = 12 (*Bhlhe40*^fl/fl) and n = 26 (*Cd23*-Cre *Bhlhe40*^fl/fl; C); n = 11 (*Bhlhe40*^fl/fl) and n = 22 (*Aicda*-Cre *Bhlhe40*^fl/fl; D); and n = 11 (*Bhlhe40*^fl/fl) and n = 16 (*Cd4*-Cre *Bhlhe40*^fl/fl; E) mice. Fold-changes are indicated. Gating on CD19⁺ and CD4⁺ lymphocytes was applied for analysis of GC B cells and T$_{FH}$ cells, respectively. **(F and G)** Flow cytometric analysis and quantification of regulatory T (T reg; F) and T$_{FR}$ (G) cells in unchallenged 14–15-wk-old WT (*Bhlhe40*^+/+ and *Bhlhe40*^fl/fl), *Bhlhe40*^−/−, and *Cd4*-Cre *Bhlhe40*^fl/fl mice. All cells shown were gated on CD4⁺ T cells. Pooled data from two independent experiments with n = 21 (WT), n = 16 (*Bhlhe40*^−/−), and n = 16 (*Cd4*-Cre *Bhlhe40*^fl/fl) mice. Mean values are shown with SD, and the data were analyzed with unpaired two-tailed Student's t test. **, P < 0.01; ***, P < 0.001; ****, P < 0.0001. One dot represents one mouse.

cycle (G2M checkpoint, E2F target genes, and mitotic spindle) in the KO T cells (Fig. 5, E and F). At least some of these genes (*E2f7*, *E2f8*, *Foxm1*, *Aurkb*, and many others) are likely to be directly repressed by Bhlhe40 in WT T cells, as evidenced by the binding of Bhlhe40 in the proximity of these genes (Figs. 5 F and S5 E) in a ChIP-seq dataset from in vitro activated CD4 T cells (Huynh et al., 2018). More genes were up-regulated than down-regulated in the KO cells (82 versus 19 genes with an adjusted P value <0.1, fold-change ≥2), in line with the notion that Bhlhe40 functions predominantly as a transcriptional repressor (Ow et al., 2014). Importantly, no change in the expression of known positive or negative regulators of T$_{FH}$ cell development and function (such as *Bcl6*, *Prdm1*, *Irf4*, *Maf*, *Batf*, *Foxo1*, or *Rc3h1*) was observed (Fig. S5 F). As Bhlhe40 recently emerged as an important regulator of cytokine production in different T cell subsets (Huynh et al., 2018; Kanda et al., 2016; Lin et al., 2014; Yu et al., 2018), we also checked the expression of genes encoding these cytokines in our T$_{FH}$-dominated antigen-specific T cells, but did not observe any change in their expression in the KO cells (Fig. S5 F). We conclude that Bhlhe40 negatively regulates T$_{FH}$ cell expansion, at least in part through the direct repression of cell cycle–related genes.

Lymphomagenesis in Bhlhe40-deficent mice

GCs are thought to be the site of origin of the majority of mature human B cell lymphomas (Basso and Dalla-Favera, 2015). We therefore next tested if dysregulation of multiple aspects of the GC reaction in *Bhlhe40*^−/− mice could ultimately lead to lymphomagenesis. Indeed, by 20 mo of age, nearly all tested *Bhlhe40*^−/− mice succumbed to a fatal disease manifested by the formation of ectopic lymphocyte-containing nodules in a variety of organs (Fig. 6, A–C) and splenomegaly. While splenomegaly has been observed in previous studies and was attributed to autoimmunity-associated lymphoproliferation (Miyazaki et al., 2010; Sun et al., 2001), ectopic lymphocyte nodules have not been reported to date, likely because younger mice were analyzed in earlier studies. Flow cytometry revealed a heterogeneous cellular composition of these nodular structures with the presence of CD4 and CD8 T cells, as well as B cells (Fig. 6 D). Strikingly, the majority of these B cells had a GC B cell phenotype, and a large fraction of CD4 T cells expressed markers of T$_{FH}$ cells (Fig. 6 E). In line with their likely GC origin, both populations expressed Bcl6 (Fig. 6 E), and the GC B-like cells expressed *Aicda* (Fig. S5 G); however, the GC architecture was not preserved in the nodules, and FDC clusters were absent (Fig. 6 F). T$_{FH}$-like cells in these structures were highly polyclonal (Fig. 6 G), while the GC B-like cells, in stark contrast to their normal WT or *Bhlhe40*-deficient counterparts, were

dominated by a single clone, as evidenced by the predominant utilization of single *Igh* and *Igk* V gene segments as revealed by RNA-seq (Fig. 6 H and data not shown). Expression of exons encoding IgH constant regions suggested that five of seven lymphomas subjected to RNA-seq originated from Ig class-switched cells (Figs. 6 I and S5 H). Interestingly, two of these lymphomas expressed the *Igha* constant region (Fig. S5 H). These results are consistent with a model in which the increased GC B cell compartment of *Bhlhe40*^−/− mice enhances the probability for malignant transformation of a B cell clone, while the expanded T$_{FH}$ cells may represent a component of the tumor stroma. Of note, a similar cellular composition in tumors, with transformed B cells being outnumbered by T cells, has been reported for several human GC-derived B cell lymphomas (Cheng and O'Connor, 2017; Scott and Gascoyne, 2014). To test if these B cells are indeed malignantly transformed and if they depend on the presence of T$_{FH}$-like cells, we transferred sorted B and CD4 T cells from diseased mice separately or in combination into *Rag2*^−/− recipients. These experiments demonstrated that B cells were required and sufficient to transfer the disease (Fig. 6 J). Notably, the presence of T$_{FH}$-like cells did not accelerate disease progression, indicating that, at least at this late stage, the transformed GC B-like cells do not depend on T cell help. We conclude that the dysregulation of the GC reaction observed in Bhlhe40-deficient mice culminates in the formation of a GC-derived B cell lymphoma.

Discussion

An efficient immune response to pathogens and vaccines relies on the interplay between two specialized lymphocyte subsets—GC B cells and T$_{FH}$ cells—that takes place in the course of the GC reaction. Intriguingly, a number of transcriptional regulators have cell-intrinsic functions in both of these cell types. While many positive regulators of GC B cells and T$_{FH}$ cells have been identified to date, little is known about the negative regulation of the GC reaction. In this study, we identified the transcription factor Bhlhe40 as a novel common negative regulator of both the B and T cell sides of the GC reaction. Regulation of two very different cell types involved in the same process by highly overlapping sets of transcription factors seems rather unusual, and reasons for this overlap remain unclear. It is interesting to note that many of these shared transcription factors, including Bhlhe40, are rapidly up-regulated upon BCR and TCR signaling and therefore seem to represent a conserved early response program downstream of both antigen receptors. The fact that the GC reaction, as well as the events preceding the formation of GCs, relies on recurrent antigen receptor signaling
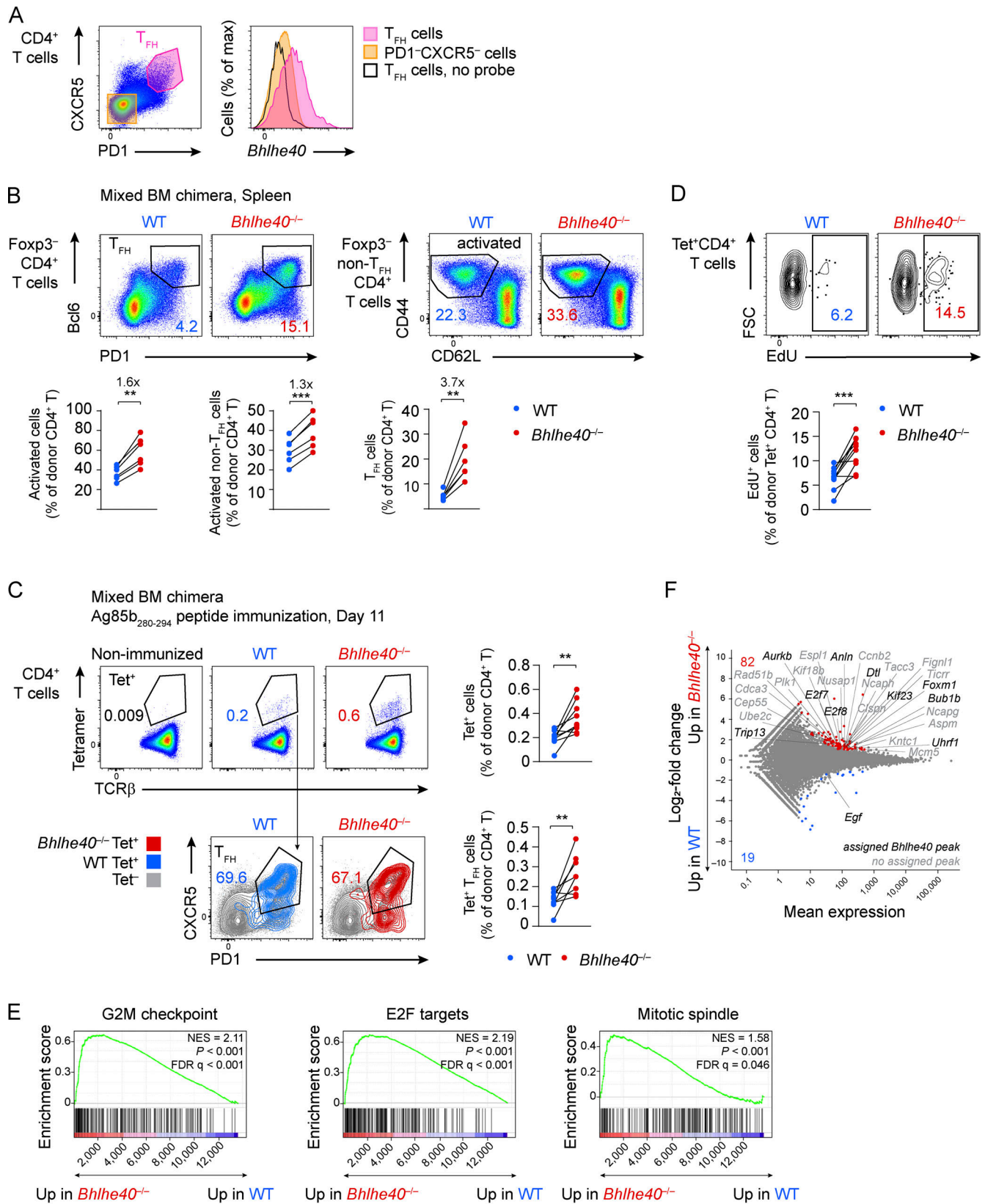
Figure 5. **Bhlhe40 limits the proliferation of T$_{FH}$ cells. (A)** *Bhlhe40* expression in T$_{FH}$ cells among CD4$^+$ T cells from spleens of unchallenged WT mice as analyzed by RNA flow cytometry. One experiment with pooled data from n = 2 mice is shown. Representative of two independent experiments. **(B)** Mixed BM chimeras were generated by transferring a 1:1 mixture of WT (CD45.1$^+$) and *Bhlhe40$^{-/-}$* (CD45.2$^+$) BM progenitor cells into lethally irradiated *Rag2$^{-/-}$* recipients. Mice were analyzed >6 wk after transfer. Expression of PD1 and Bcl6 by WT and *Bhlhe40$^{-/-}$* Foxp3$^-$CD4$^+$ T cells (top row, left), flow cytometric analysis of activated CD44$^+$CD62L$^-$ cells among WT and *Bhlhe40$^{-/-}$* Foxp3$^-$ non-T$_{FH}$ CD4$^+$ T cells (top row, right), and quantification among total WT and *Bhlhe40$^{-/-}$*

Rauschmeier et al.
Bhlhe40 in the germinal center reaction

Journal of Experimental Medicine   11 of 21
https://doi.org/10.1084/jem.20211406

Foxp3⁻CD4⁺ T cells in the spleen (bottom row). For quantification, T$_{FH}$ cells were gated as Foxp3⁻Bcl6⁺CD4⁺ T cells or Foxp3⁻Bcl6⁺PD1⁺CD4⁺ T cells (T$_{FH}$ of donor CD4⁺ T). Fold-changes are indicated. One experiment with n = 6 mice is shown. Representative of two independent experiments. **(C–F)** Mixed BM chimeras were generated by transferring a 1:1 mixture of WT (CD45.1⁺/CD45.2⁺) and $Bhlhe40^{−/−}$ (CD45.1⁺) BM progenitor cells into lethally irradiated WT (CD45.2⁺) recipients. Mice were immunized with *M. tuberculosis* Ag5b$_{280-294}$ peptide emulsified in complete Freund's adjuvant >7 wk after transfer. **(C)** Flow cytometric analysis and quantification of Ag85b-tetramer–binding CD4⁺ T cells and T$_{FH}$ cells among WT and $Bhlhe40^{−/−}$ CD4⁺ T cells in the spleen on day 11 after immunization. **(D)** Immunized mixed BM chimeras were i.p. injected with EdU 18 and 14 h before harvest on day 11. EdU incorporation by Ag85b-tetramer–binding WT and $Bhlhe40^{−/−}$ CD4⁺ T cells is shown. One experiment with n = 9 (C) and n = 10 (D) mice is shown. Representative of two independent experiments each. Data were analyzed with paired two-tailed Student's t test (B–D). NS, P > 0.05; **, P < 0.01; ***, P < 0.001. One dot represents one mouse. **(E and F)** RNA-seq analysis of Ag5b-tetramer–binding WT and $Bhlhe40^{−/−}$ CD4⁺ T cells isolated from mixed BM chimeras 11 d after immunization. **(E)** GSEA showing three most enriched gene sets from MSigDB Hallmark collection. G2M checkpoint, E2F target and mitotic spindle genes depicting the change in their expression in $Bhlhe40^{−/−}$ relative to that in WT Ag85b-tetramer–binding CD4⁺ T cells. FDR, false discovery rate; NES, normalized enrichment score. **(F)** Comparison of changes in gene expression induced by Bhlhe40 deficiency in Ag85b-tetramer–binding CD4⁺ T cells. Log$_2$ fold-changes between $Bhlhe40^{−/−}$ and WT CD4⁺ T cells are plotted, and the significantly (more than twofold, adjusted P < 0.05) up- and down-regulated genes are indicated. Cell cycle–related genes (GO:0007049) that significantly (twofold or more, adjusted P < 0.1) changed their expression in $Bhlhe40^{−/−}$ cells are highlighted. Gene names in bold correspond to genes with assigned Bhlhe40 ChIP-seq peaks.

events in both GC B cells and T$_{FH}$ cells could explain why some of the induced early response genes may be expressed and functional in both subsets. Of note, most of the transcription factors shared by GC B and T$_{FH}$ cells are not exclusively involved in the regulation of only B and T cell subsets participating in the GC reaction. This applies to Bhlhe40, which regulates cytokine production in a variety of T cell subsets (Huynh et al., 2018; Kanda et al., 2016; Lin et al., 2014; Yu et al., 2018) and, together with Bhlhe41, contributes to regulation of the development and self-renewal of B-1a B cells (Kreslavsky et al., 2017). It is also conceivable that shared regulators of the GC reaction could in some cases represent a convenient "switch" that would allow the enhancement or dampening of both the B and T cell sides of the GC response upon exposure to the same upstream signals. Indeed, one could envision that if Bhlhe40 could be up- or down-regulated in both B and T lymphocytes, for example by a common cytokine, which would allow simultaneous negative or positive regulation of both main lymphocyte types involved in the GC reaction.

Although Bhlhe40 recently emerged as an important regulator of cytokine production by T cells (Huynh et al., 2018; Kanda et al., 2016; Lin et al., 2014; Yu et al., 2018), Bhlhe40-deficient antigen-specific CD4 T cells did not exhibit changes in the expression of cytokine-encoding genes in response to immunization conditions that favor T$_{FH}$ cell differentiation as used in our study. We also did not observe dysregulation of expression of mitochondria-related genes, which was described for Bhlhe40-deficient tissue-resident memory CD8 T cells (Li et al., 2019). Instead, activated Bhlhe40-deficient CD4 T cells in our experiments up-regulated cell cycle–related genes and exhibited increased proliferation. This is in line with several reports that suggest that Bhlhe40 and Bhlhe41 may have a mild cytostatic function in a variety of cellular contexts (Ow et al., 2014). As we also previously observed antiproliferative effects of these transcription factors in B-1a cells (Kreslavsky et al., 2017), we initially hypothesized that Bhlhe40 also restrained proliferation of early GC B cells or their immediate precursors. However, extensive in vivo and in vitro experiments failed to reveal any evidence for an antiproliferative function of Bhlhe40 in activated B cells. The earliest GC B cells also exhibited remarkably low levels of apoptosis, and no change in frequency of apoptotic cells was observed between WT and KO cells. Moreover, while Bhlhe40 was expressed in the highly proliferative CCR6⁺

common activated precursors of early MBCs, PBs, and GC B cells, only the latter population was selectively affected by Bhlhe40 deficiency. Taken together, these results suggested that Bhlhe40 negatively regulates GC B cell development. In line with this notion, analysis of GC B cell differentiation trajectory by scRNA-seq indicated that Bhlhe40-deficient B cells gained a competitive advantage at the earliest steps of GC B cell differentiation. Moreover, Bhlhe40-deficient activated B cells exhibited a mild up-regulation of GC B cell signature genes, suggesting that they may be more prone to adopt the GC B cell fate. Taken together, these results suggest that Bhlhe40 restrains the generation of the earliest cells seeding the GC reaction. Interestingly, a published scRNA-seq analysis of human tonsillar B lymphocytes revealed the highest level of *BHLHE40* expression in an activated B cell subset suggested to represent the immediate precursors of GC B cells (King et al., 2021). This observation suggests that the role of this transcription factor in activated B cells may be conserved between primates and rodents.

The negative regulation of early GC B cell generation, revealed through loss-of-function experiments in this study, would suggest that overexpression of Bhlhe40 should interfere with the GC reaction. Indeed, the transgenic overexpression of *Bhlhe40* driven by the V$_H$ promoter and the Eμ enhancer was previously shown to impair the generation of GC B cells upon immunization (Seimiya et al., 2004), complementing our loss-of-function analysis.

Although $Bhlhe40^{−/−}$ B cells did not exhibit altered levels of Bcl6 expression, the GC B cell phenotype of Bhlhe40 deficiency was highly reminiscent of that observed in IμBcl6 transgenic mice. Compared with WT B cells, activated IμBcl6-transgenic B cells exhibited a 25% up-regulation of Bcl6 protein expression already starting at the earliest stages of GC B cell differentiation (Robinson et al., 2020). This mild overexpression resulted in a competitive advantage of the transgenic cells selectively in the GC B cell compartment in the first days of the response but, very similarly to Bhlhe40 deficiency, did not affect fitness of the cells at later time points (Robinson et al., 2020). With age, IμBcl6 animals developed a lymphoma of GC B cell origin (Cattoretti et al., 2005).

Dysregulation of the GC reaction in Bhlhe40-deficient mice likewise culminated in the development of a GC B cell lymphoma. Cellular composition of these lymphomas strongly
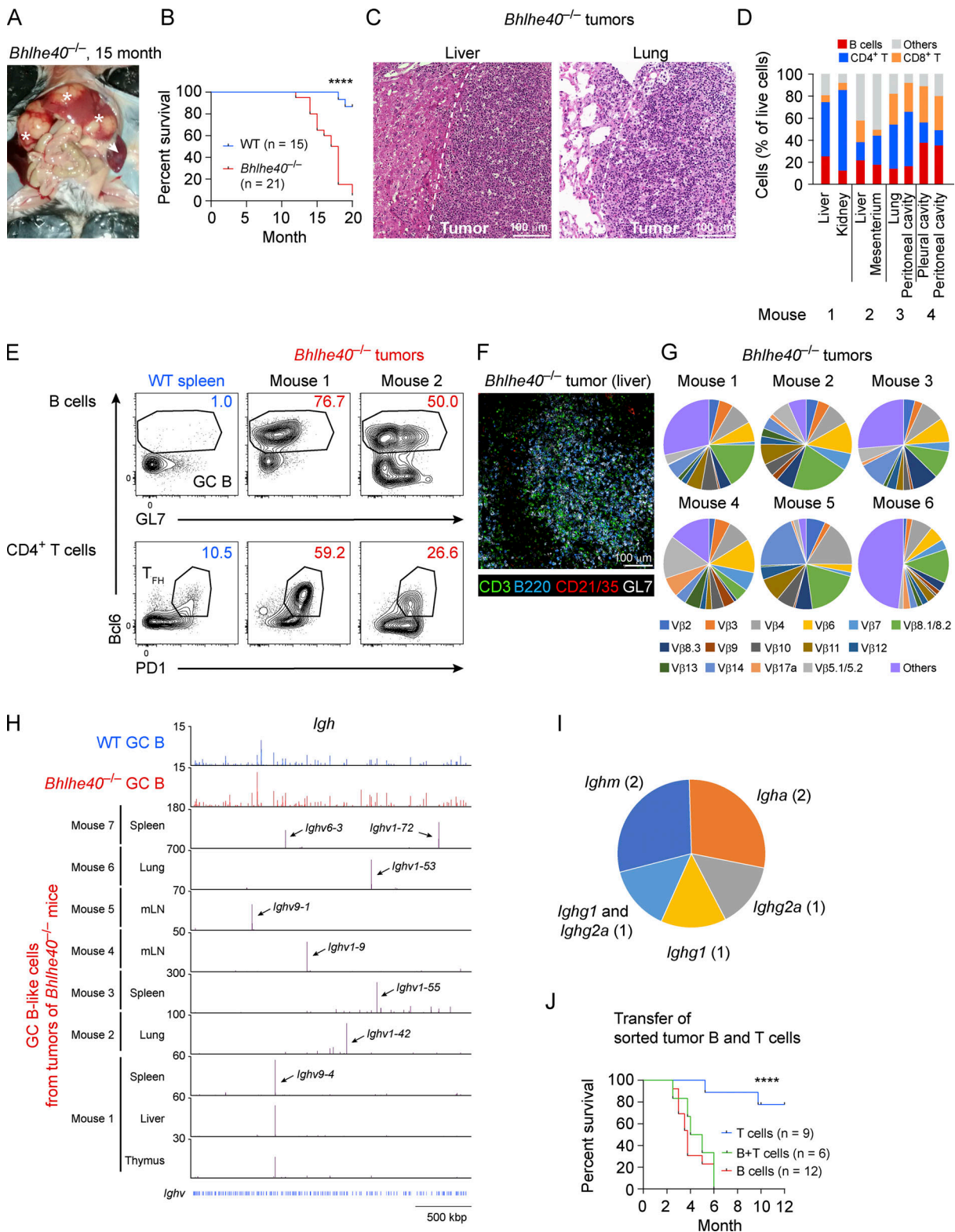
Rauschmeier et al.
Bhlhe40 in the germinal center reaction

Journal of Experimental Medicine
https://doi.org/10.1084/jem.20211406

12 of 21

Figure 6. **Lymphomagenesis in aging *Bhlhe40*⁻/⁻ mice. (A)** Image of a 15-mo-old *Bhlhe40*⁻/⁻ mouse demonstrating splenomegaly (arrow) and nodular structures (asterisks) in the liver. **(B)** Kaplan–Meier survival curve depicting the survival of aging WT and *Bhlhe40*⁻/⁻ mice. Pooled data for WT (*n* = 15) and *Bhlhe40*⁻/⁻ (*n* = 21) mice. **(C)** H&E staining of sections of nodules in the liver and lung from two 15-mo-old *Bhlhe40*⁻/⁻ mice. **(D)** Quantification of the composition of nodules of sick *Bhlhe40*⁻/⁻ mice as assessed by flow cytometry. **(E)** Flow cytometric analysis of GL7, PD1, and Bcl6 expression in the CD19⁺ B cell and CD4⁺ T cell populations of an age-matched WT spleen and tumors from sick *Bhlhe40*⁻/⁻ mice between 15 and 18 mo of age. Data are representative of 12 sick *Bhlhe40*⁻/⁻ mice analyzed. **(F)** Representative image of a tumor nodule section from the liver of a sick *Bhlhe40*⁻/⁻ mouse. Cells expressing CD3 (green), B220 (blue), CD21/CD35 (red), and GL7 (white). Data are representative of three analyzed mice. **(G)** TCRβ V segment usage by T_FH-like cells from nodules of sick *Bhlhe40*⁻/⁻ mice as determined by flow cytometry. **(H and I)** RNA-seq analysis of GC B-like lymphoma cells isolated from the indicated organs of sick *Bhlhe40*⁻/⁻

Rauschmeier et al.
Bhlhe40 in the germinal center reaction

Journal of Experimental Medicine   13 of 21
https://doi.org/10.1084/jem.20211406

mice (mice 1, 2, 4–7) or sick *Rag2*⁻/⁻ recipient of *Bhlhe40*⁻/⁻ lymphoma cells (mouse 3). **(H)** Genome browser view indicating the expression of V gene segments in the *Igh* locus. **(I)** Pie chart showing the expression of the predominantly used *Igh* constant region by *Bhlhe40*⁻/⁻ lymphomas (primary data shown in Fig. S5 H). The number of tumors expressing the indicated *Igh* constant region is shown in brackets. **(J)** Kaplan–Meier survival curve depicting the survival of *Rag2*⁻/⁻ recipients that were transferred with sorted B and T cells from a sick *Bhlhe40*⁻/⁻ mouse. Pooled data from two independent experiments performed with the indicated mice transplanted with B cells (*n* = 12), T cells (*n* = 9), and B + T cells (*n* = 6) are shown. Log-rank (Mantel–Cox) test was used (B and J). ****, P < 0.0001.

suggests that dysregulation of the GC reaction underlies the disease. However, the relative contribution of B cell– and T_{FH} cell–intrinsic aspects of the *Bhlhe40* KO phenotype to lymphomagenesis, as well as possible involvement of the other cell types in the process, remains to be tested. For example, it seems probable that the age-dependent decrease in regulatory T cells observed in Bhlhe40-deficient mice (Miyazaki et al., 2010), as well as the decrease of the T_{FR}/T_{FH} cell ratio reported here, can also contribute to the lymphomagenesis.

Lymphomas in *Bhlhe40*⁻/⁻ mice took more than a year to develop, suggesting that accumulation of additional mutations in GC B cells in the course of a dysregulated GC reaction may be required for the malignant transformation. In line with this notion, RNA-seq analysis of the tumor cells demonstrated that they express *Aicda*, suggesting that lymphoma cells could continuously undergo AID-mediated mutagenesis. Indeed, expression of AID was required for formation of GC-derived lymphomas in IµBcl6 mice (Pasqualucci et al., 2008), and ectopic AID expression by itself is sufficient to drive malignant transformation (Okazaki et al., 2003). It is thus conceivable that Bhlhe40 prevents lymphomagenesis not through a direct tumor suppressor function, but by restraining the GC reaction as such, therefore reducing the numbers of cells prone to malignant transformation. Expression of the *Igha* constant region by two of the tumors analyzed by RNA-seq suggests that some lymphomas may have originated from an IgA-switched cell from a "chronic" GC in mucosal lymphoid tissue. While it remains to be seen if Bhlhe40 mutations can be found in human B cell lymphomas, the unusual cellular composition of the lymphomas in Bhlhe40-deficient mice is reminiscent of certain human malignancies. The highly heterogeneous cellular composition of the nodules in diseased *Bhlhe40*⁻/⁻ mice contrasts with the dominance of transformed B cells in the case of human follicular lymphoma, GC B cell–like diffuse large B cell lymphoma, and Burkitt's lymphoma, and the normal GC B cell phenotype of the cells is inconsistent with classical Hodgkin's lymphomas. However, the observed phenotype has intriguing similarities to human T cell/histiocyte-rich large B cell lymphoma and nodular lymphocyte-predominant Hodgkin's lymphoma, since in both conditions, transformed Bcl6-positive GC B cells are outnumbered by T cells (Cheng and O'Connor, 2017; Scott and Gascoyne, 2014). Of note, the etiology of these human lymphomas is not well understood, and it remains unknown what mutations lead to malignant transformation in these cases.

Taken together, the results reported in this study identify the transcription factor Bhlhe40 as a novel cell-intrinsic negative regulator of both the B and T cell sides of the GC reaction, expression of which is crucial to prevent lymphomagenesis.

Materials and methods

Mice

All mice used in this study were maintained on the C57BL/6 genetic background. The *Igh*^B1-8hi (Shih et al., 2002), *Bhlhe40*⁻/⁻ (Sun et al., 2001), *Bhlhe41*⁻/⁻ (Rossner et al., 2008), *Rag2*⁻/⁻ (Shinkai et al., 1992), *Mb1*-Cre (Hobeika et al., 2006), *Cd4*-Cre (Lee et al., 2001), *Cd23*-Cre (Kwon et al., 2008), *Aicda*-Cre (Kwon et al., 2008), *Vav1*-Cre (de Boer et al., 2003), and *Rosa26*-LSL-YFP (Srinivas et al., 2001) mice were described previously. *Bhlhe40*^fl/fl mice were generated as described below. WT C57BL/6J mice were obtained from Janvier Labs or bred in-house. Mice analyzed in this study were at least 6 wk old and kept under specific pathogen–free conditions. Mice were bred and maintained at the Comparative Medicine Biomedicum facility of Karolinska Institutet (Stockholm, Sweden) or at the Research Institute for Molecular Pathology (Vienna, Austria). All mouse experiments were performed according to valid project licenses, which are approved and regularly controlled by the Swedish and/or Austrian Veterinary Authorities.

Generation of *Bhlhe40*^fl/fl mice

Bhlhe40^fl mice were generated by CRISPR-Cas9–mediated genome editing in mouse zygotes (Yang et al., 2013). A solution containing two sgRNAs targeting *Bhlhe40* sequences in introns 2 and 4 (Fig. S5 A), Cas9 mRNA, Cas9 protein, and single-strand DNA repair template was injected into C57BL/6 × CBA zygotes. Correct targeting was confirmed by sequencing, and the mice were backcrossed to the C57BL/6 genetic background for four generations before crossing them to the Cre lines.

Flow cytometry

Mouse organs were harvested, and single-cell suspensions were obtained by mincing through 70-µm cell strainers. For detection of antigen-specific CD4 T cells, splenic single-cell suspensions were incubated with APC-conjugated I-A^b Mtb Ag85b$_{280-294}$ and I-A^b 2W1S tetramers (provided by National Institutes of Health Tetramer Core Facility) for 1 h before Fc receptor blocking and further cell surface staining. For detection of PE-specific B cells in the polyclonal response in mice, splenic single-cell suspensions were incubated in IMDM (Thermo Fisher Scientific), pH 3.0, on ice for 1 min to remove Fc receptor–bound antibodies, washed twice with PBS/2% FCS, and stained with PE (Prozyme, 20 µg/ml).

RNA flow cytometry measurement of *Bhlhe40* expression was performed using the PrimeFlow RNA Assay (Thermo Fisher Scientific) according to the manufacturer's instructions. High-sensitivity Alexa Fluor 647 probes were used. Intracellular staining for cleaved caspase-3 was performed using the 5A1E rabbit monoclonal antibody, Alexa Fluor 647–labeled anti-rabbit

F(ab)₂ fragment (both from Cell Signaling Technology), and the Cytofix/Cytoperm kit (BD Biosciences) according to the manufacturer's instructions. Intracellular staining for transcription factors was performed using the Foxp3 staining buffer set (Thermo Fisher Scientific) according to the manufacturer's instructions. Detection of cells positive for EdU was performed using the Click-iT Plus EdU A488 or Click-iT Plus Pacific Blue Flow Cytometry Assay Kit (Thermo Fisher Scientific) following the manufacturer's instructions with minor modifications. Data were acquired on an LSR Fortessa Flow Cytometer (BD Biosciences) and analyzed with FlowJo software v10 (BD Biosciences).

Antibodies
For staining of murine samples, monoclonal antibodies specific for BCL6 (REA373 and K112-91), IRF4 (3E4), CD4 (GK1.5, RM4-8, and S11), CD3e (145-2C11, 17A2, and REA641), CD8 (53-6.7 and YTS156.7.7), PD-1 (RMP1-30, REA802, and 29F.1A12), CXCR5 (2G8 and REA215), CD44 (IM7), CD62L (MEL-14), CD19 (1D3 and 6D5), B220 (RA3-6B2), GL7 (GL7), CD95 (JO2 and REA453), CCR6 (REA277 and 29-2L17), CD38 (90), CD138 (REA104 and 281–2), TACI (8F10), CD86 (GL1), CXCR4 (2B11), IgM (REA979 and RMM-1), IgD (11-26c2a), IgG1 (REA1017 and RMG1-1), Igλ (R26-46 and JC5-1), CD21/CD35 (7E9), CD45.1 (A20 and REA1179), CD45.2 (104 and 104-2), Igκ (187.1), Gr-1 (RB6-8C5), F4/80 (BM8), CD11c (HL3 and N418), CD11b (M1/70), Ly6G (1A8), NK1.1 (PK136), TCRβ (H57-597 and REA318), TCRγδ (GL3), and Ter119 (Ter119) were purchased from BioLegend, BD Biosciences, Miltenyi Biotec, or Thermo Fisher Scientific and were used at dilutions specified by the manufacturer or determined experimentally. For staining for TCRβ subtypes in Bhlhe40⁻/⁻ tumor mice, the mouse Vβ TCR screening panel (BD Bioscience) was used.

Generation of mixed BM chimeras and adoptive cell transfers
BM cells from WT and Bhlhe40⁻/⁻, Bhlhe41⁻/⁻, or Bhlhe40⁻/⁻Bhlhe41⁻/⁻ mice were stained with CD4, CD8, CD3, TCRβ, TCRγδ, NK1.1, CD19, CD11b, CD11c, Gr-1, and Ter119 APC- or PE-labeled antibodies followed by magnetic depletion with anti-APC or -PE Micro-Beads (Miltenyi Biotec), respectively. WT and KO cells were mixed at a 1:1 ratio (unless stated otherwise) and 2–4 × 10⁶ cells were transferred i.v. into lethally irradiated (split dose: 500 rads, twice) WT or Rag2⁻/⁻ recipients (as indicated). CD45.1 and CD45.2 congenic markers were used as indicated. Chimeras were analyzed >6 wk after reconstitution.

For adoptive transfer experiments, splenocytes from congenically distinguishable Bhlhe40⁺/⁺ Igh^B1-8hi/⁺ and Bhlhe40⁻/⁻ Igh^B1-8hi/⁺ mice were mixed targeting a 1:1 ratio of WT and Bhlhe40⁻/⁻ cells in the antigen-specific B cell compartment (CD19⁺Igλ⁺). The ratio was confirmed by flow cytometric analysis of an aliquot from the mix and adjusted when necessary. 10–14 × 10⁶ of splenocytes (~3–5 × 10⁵ NP-specific B cells counting both donors together) were injected into the tail vein of congenically distinguishable sex-matched C57BL/6 recipient mice. Recipient mice were immunized 12–24 h after transfer as described below. To analyze the distribution of WT (Cd23-Cre Rosa26-LSL-YFP) and Bhlhe40⁻/⁻ (CD45.1⁺) Igλ⁺ B1-8hi B cells on days 2 and 4 after immunization, sorted RBC-depleted Igκ⁻lin⁻ WT (YFP⁺) and Bhlhe40⁻/⁻ (CD45.1⁺) splenocytes were mixed targeting a 1:1 ratio of WT and Bhlhe40⁻/⁻ cells in the antigen-specific B cell compartment as described above. 6 × 10⁵ NP-specific B cells were intravenously injected 1 d before immunization.

For adoptive transfer of B and T cells from Bhlhe40⁻/⁻ tumor mice, CD19⁺ B cells and CD4⁺ T cells were sorted from the spleens of sick Bhlhe40⁻/⁻ tumor mice using a Sony SH800 Cell Sorter. More than 5 × 10⁵ B cells and/or T cells were transferred i.v. into congenically distinguishable sex-matched Rag2⁻/⁻ recipient mice via injection into the tail vein.

Immunizations experiments
For B1-8hi transfer experiments, C57BL/6 recipient mice were preimmunized by i.p. injection of 100 µg OVA (BioSearch Technologies) dissolved in PBS and precipitated in alum (Sigma-Aldrich) at a 1:1 ratio >2 wk before adoptive cell transfer. 12–24 h after B1-8hi cell transfer, recipient mice were immunized by i.p. injection of 100 µg NP₁₉-OVA (BioSearch Technologies) precipitated in alum (Sigma-Aldrich) at a 1:1 ratio. For NP-Ficoll immunization, non-preimmunized C57BL/6 recipient mice were i.p. injected with 100 µg NP₄₆-Ficoll (BioSearch Technologies) dissolved in PBS and precipitated in alum at a 1:1 ratio. For in vivo proliferation analysis, 1 mg EdU (Sigma-Aldrich) diluted in PBS was i.p. or i.v. injected at indicated time points after immunization. For PE immunization, mice were s.c. injected with 50 µl of an emulsion containing 50 µg of PE. Emulsions were prepared by mixing PE in PBS in a 1:1 ratio with complete Freund's adjuvant (Sigma-Aldrich). For peptide immunizations, mice were i.p. injected with 100 µg Ag85b₂₈₀₋₂₉₄ (FQDAY-NAAGGHNAVF) or 2W1S (EAWGALANWAVDSA) peptide in 100 µl of a 1:1 emulsion with complete Freund's adjuvant.

Quantitative RT-PCR (qRT-PCR)
WT splenic naive B cells were isolated using depletion with CD43 Micro-Beads (Miltenyi Biotec) and stimulated with anti-CD40 (1 µg/ml; HM40-3; Invitrogen) or polyclonal anti-IgM F(ab')₂ (1 µg/ml; Jackson ImmunoResearch) antibody alone or in combination with IL-4 (20 ng/ml, Peprotech) for the indicated time. Total RNA was isolated from cultured B cells using the Quick-RNA Microprep Kit (Zymo Research). cDNA was synthesized with the RevertAid RT Kit (Thermo Fisher Scientific), and qRT-PCR was performed on a CFX96-C1000 Thermo Cycler (Bio-Rad) using the SensiFAST SYBR No-ROX Kit (Bioline; Meridian Bioscience). Hprt1 was used as a housekeeping gene, and the standard curve method was used for quantification. The following primers were used: Bhlhe40-F, 5′-CTCCTACCCGAACATCTCAAAC-3′, Bhlhe40-R, 5′-CCAGAACCACTGCTTTTTCC-3′, Hprt1-F, 5′-AGTGTTGGATACAGGCCAGAC-3′, and Hprt1-R, 5′-CGTGATTCAAATCCCTGAAGT-3′.

In vitro proliferation
WT and Bhlhe40⁻/⁻ splenic naive B cells were isolated using depletion with CD43 Micro-Beads (Miltenyi Biotec), mixed in a 1:1 ratio and subsequently labeled using the CellTraceViolet Proliferation Kit (Thermo Fisher Scientific). Up to 50 × 10⁶ splenocytes were incubated in 1 ml prewarmed PBS/0.1% BSA with 2.5 µM CellTrace Violet reagent for 8 min at 37°C. The reaction was stopped with FCS. Naive CD43⁻ B cells were stimulated with

Rauschmeier et al.
Bhlhe40 in the germinal center reaction

Journal of Experimental Medicine   15 of 21
https://doi.org/10.1084/jem.20211406

the indicated concentrations of anti-CD40 (HM40-3; Invitrogen) or anti-IgM F(ab')$_2$ (Jackson ImmunoResearch) antibody alone or in combination with IL-4 (20 ng/ml, Peprotech) for 3 d.

ELISPOT assay

The numbers of NP-specific IgG1 ASCs in the BM of NP-OVA–immunized WT and *Bhlhe40*$^{-/-}$ mice 26 d after immunization were determined by ELISPOT assay. To this end, MAIPSWU10 96-well plates (Millipore) were coated overnight at 4°C with 5 μg/ml NP$_{25}$-BSA (BioSearch Technologies) in PBS. RBC-depleted BM cells were plated in duplicate threefold dilution series from 10^6 to 1.23 × 10^5 cells per well and incubated overnight at 37°C in RPMI supplemented with 10% FCS, 1% L-glutamine, 1% penicillin-streptomycin, and 0.1% β-mercaptoethanol. Plates were washed with PBS/0.05% Tween-20 and subsequently incubated with 1 μg/ml biotinylated anti-mouse IgG1 antibody (RMG1-1; BioLegend). Spots were visualized with alkaline phosphatase–conjugated streptavidin (Mabtech) and BCIP-NBT-plus substrate (Mabtech). Plates were extensively washed, spots were counted using an AID ELISpot Reader (AID Diagnostika), and the mean cell number of NP-specific IgG1 ASCs per 10^6 BM cells was calculated from each threefold dilution series.

H&E staining

Tissue samples of liver and lung from *Bhlhe40*$^{-/-}$ tumor mice were processed using the standard tissue protocol on an Automatic Tissue Processor Donatello (Diapath) and embedded in paraffin. 2-μm paraffin sections were cut. Sections were rehydrated with xylene substitute (Thermo Fisher Scientific) and ethanol, followed by staining with H&E (both Thermo Fisher Scientific) for 1 min each and again dehydrated with ethanol and xylene substitute. After embedding in aqueous mounting medium (Eukitt Neo), slides were analyzed using a Pannoramic FLASH 250 III slide scanner equipped with an Adimec Quartz Q12A180 camera.

Immunofluorescence microscopy

For confocal immunofluorescence microscopy, organs were harvested, fixed in 4% PFA in PBS for 1–2 h, and subsequently incubated in 30% sucrose in PBS for up to 3 h. Organs were embedded in Tissue Tek Optimal Tissue Cutting Temperature medium (OCT; Sakura Finetek) and snap frozen on dry ice. 8-μm sections were cut using a cryostat, and sections were mounted on SuperFrost Plus glass slides (Thermo Fisher Scientific). Sections were incubated in ice-cold acetone for 10 min before blocking in 5% BSA in PBS. To block endogenous biotin, the streptavidin/biotin blocking kit (Vector Laboratories) was used according to the manufacturer's instructions. Staining was performed for 1 h at RT in a humidified chamber, and slides were mounted with Fluoromount Aqueous Mounting Medium (Sigma-Aldrich). For YFP detection, slides were incubated with Alexa Fluor 488–conjugated GFP booster (Chromotek), and staining was performed according to the manufacturer's instructions. Confocal images were acquired on an LSM 700 system (Carl Zeiss) with 405-, 488-, 555-, and 639-nm excitation lines at the Biomedicum Imaging Core at the Karolinska Institute. Images were processed using Zen 2.3 Black Edition

(Carl Zeiss) or Imaris (Bitplane) imaging software, and only minor changes for individual color channel adjustment were performed.

To analyze the size of the GCs in spleen sections of untreated WT and *Bhlhe40*$^{-/-}$ mice, samples were prepared and imaged as described above. Additional images were acquired using a Pannoramic 250 Flash Slide Scanner equipped with a 20× objective (3DHISTECH). GCs were identified as IgD-negative areas within B cell follicles, and CaseViewer (3DHISTECH) or ImageJ software was used to measure the size of the GCs. To compare the distribution of sorted Igκ$^-$lin$^-$ WT and *Bhlhe40*$^{-/-}$ B1-8^{hi} B cells in the spleen on days 2 and 4 after immunization, the perimeter and GC area of each analyzed follicle was identified by CD169 and GL7 staining, respectively. To quantify the frequency of cells in the CD169$^+$ follicle perimeter, all WT (YFP$^+$) and *Bhlhe40*$^{-/-}$ (CD45.1$^+$) cells located within the perimeter and inside the B cell follicle were counted (excluding cells already located within GCs) using ImageJ software.

ChIP-seq analysis of Bhlhe40 binding

WT splenic naive B cells were isolated using CD43 Micro-Beads (Miltenyi Biotec) and stimulated with 1 μg/ml anti-CD40 antibody (HM40-3; Invitrogen) for 4 h. Cells were fixed with 1% PFA in PBS in the presence of 1% FCS at RT. Fixation was stopped after 10 min by addition of glycine in PBS (final concentration 0.1 M). Cells were washed with 0.1 M glycine solution in PBS. Live CD19$^+$ cells were sorted, and pellets were frozen. ChIP and library preparation were performed as recently described (Gustafsson et al., 2018), with minor modifications. 3 × 10^6 and 22 × 10^6 fixed frozen B cells were thawed at room temperature and diluted with SDS lysis buffer (50 mM Tris/HCl, pH 8, 0.5% SDS, and 10 mM EDTA, pH 8) containing 1× cOmplete protease inhibitor. Cells were sonicated in a Bioruptor Plus sonicator (Diagenode). To neutralize the SDS, Triton X-100 was added to a final concentration of 1% along with cOmplete protease inhibitor. Samples were incubated at room temperature for 10 min. 3 μg of rabbit polyclonal anti-Bhlhe40 antibody (NB100-1800, lot C2; Novus Biologicals) was added to 10 μl protein G–coupled Dynabeads (Thermo Fisher Scientific) in PBS with 0.5% BSA and incubated with rotation for 4 h at 4°C. Antibody-coated Dynabeads were washed with PBS with 0.5% FCS and mixed with cell lysate in PCR tubes. Tubes were incubated with rotation overnight at 4°C. Immunoprecipitated chromatin was washed with 150 μl of low-salt buffer (50 mM Tris/HCl, 150 mM NaCl, 0.1% SDS, 0.1% sodium deoxycholate, 1% Triton X-100, and 1 mM EDTA), high-salt buffer (50 mM Tris/HCl, 500 mM NaCl, 0.1% SDS, 0.1% sodium deoxycholate, 1% Triton X-100, and 1 mM EDTA), and LiCl buffer (10 mM Tris/HCl, 250 mM LiCl, 0.5% IGEPAL CA-630, 0.5% sodium deoxycholate, and 1 mM EDTA), followed by two washes with TE buffer (10 mM Tris/HCl and 1 mM EDTA) and two washes with ice-cold Tris/HCl, pH 8. For tagmentation, bead-bound chromatin was resuspended in 30 μl of tagmentation buffer. 1 μl of transposase (Nextera; Illumina) was added, and samples were incubated at 37°C for 10 min followed by two washes with low-salt buffer. Bead-bound tagmented chromatin was diluted in 20 μl of water. 25 μl PCR master mix (Nextera; Illumina) and 5 μl indexed amplification

primers (Buenrostro et al., 2013; 0.125 µM final concentration) were added, and libraries were prepared using the following PCR program: 72°C for 5 min (adapter extension); 95°C for 5 min; followed by 11 cycles of 98°C for 10 s, 63°C for 30 s, and 72°C for 3 min. All steps from sonication to library amplification PCR were performed in the same PCR tube. After PCR amplification, library cleanup was done using Agencourt AmPureXP beads (Beckman Coulter) at a PCR mix/bead ratio of 1:1. DNA concentrations in purified samples were measured using the Qubit dsDNA HS Kit (Invitrogen). Libraries were sequenced single-end with 41-bp read length on a NextSeq 500 system (Illumina).

Analysis of ChIP-seq data

Bhlhe40 ChIP-seq reads from our activated B cell dataset (3×10^6 and 22×10^6 B cells), as well as a published activated CD4 T cell ChIP-seq dataset (GEO accession number GSE113054; Huynh et al., 2018) were aligned to the mouse genome assembly version of July 2007 (NCBI37/mm9), using the Bowtie2 program (Langmead and Salzberg, 2012; https://usegalaxy.eu; Galaxy v2.3.4.2 [Afgan et al., 2018]), and BAM files for 3×10^6 and 22×10^6 cell samples were merged. Peaks were called with a P value of $<10^{-10}$ with the MACS program v1.3.6.1 (Feng et al., 2012) and default parameters. The identified peaks were then assigned to target genes as described (Revilla-i-Domingo et al., 2012). Bhlhe40 peaks overlapping with the transcription start site were referred to as promoter peaks. For motif discovery, we used the MEME-ChIP suite (Machanick and Bailey, 2011; Galaxy v4.11.2 [Afgan et al., 2018]) to predict the most significant motifs present in the 300 bp centered at the peak summit of the top 500 sequences, as sorted by the fold enrichment score of the MACS program.

RNA-seq analysis

For RNA-seq analysis of activated B cell populations, congenically distinguishable WT and KO B1-8^{hi} B cells were co-transferred into OVA-preimmunized WT recipients as described above and isolated on day 4 after NP-OVA immunization. Splenocytes were depleted using Igκ/CD4/CD8/GR1/Ter119/TCRβ/TCRγδ/CD11b/CD11c/NK1.1 antibodies and anti-PE Micro-Beads (Miltenyi Biotec), and WT (CD45.1$^+$CD45.2$^-$) and KO (CD45.1$^+$CD45.2$^+$) antigen-specific (CD19$^+$Igλ$^+$) GC B cells (CCR6$^-$GL7^{hi}) or non-GC B-activated B cells (CCR6$^+$GL7^{int}) were double sorted. For the second sort, 500 cells were sorted directly into lysis buffer and subjected to the SMART-Seq v2 Cell protocol (Picelli et al., 2014). Libraries were subjected to Illumina deep sequencing (HiSeqV4 SR50).

For RNA-seq analysis of activated T cells, WT and Bhlhe40$^{-/-}$ mixed BM chimeras were generated as described above and i.p. injected with 100 µg Ag85b$_{280-294}$ peptide in 100 µl of a 1:1 emulsion with complete Freund's adjuvant. On day 11 after immunization, spleens were harvested, and single-cell suspensions were incubated with APC-conjugated I-A^b Mtb Ag85b$_{280-294}$ tetramer (provided by National Institutes of Health Tetramer Core Facility) for 1 h at 4°C. Tetramer-positive cells were enriched using anti-APC Micro-Beads (Miltenyi Biotec). CD19$^-$CD11c$^-$CD11b$^-$F4/80$^-$CD8a$^-$ WT (CD45.1$^+$CD45.2$^+$) and Bhlhe40$^{-/-}$ (CD45.1$^+$) antigen-specific T cells (Tetramer$^+$CD4$^+$TCRb$^+$) were double sorted. For the

second sort, 1,000 cells were directly sorted into 5 µl single-cell lysis solution (Invitrogen) according to the manufacturer's instructions with minor modifications, as sorted cells were incubated for 15 min in the single-cell DNase/lysis solution. cDNA and second-strand synthesis was performed using NEBNext Ultra II RNA First Strand Synthesis (E7771; NEB) and NEBNext Ultra II Directional RNA Second Strand Synthesis (E7550; NEB) modules. QIAseq FastSelect rRNA HMR kit (Qiagen) was used to minimize ribosomal RNA contribution to the final library. Custom-made Tn5 (transposase) in combination with oligo replacement and PCR amplification was used to generate indexed sequencing libraries (Gertz et al., 2012). Libraries were pooled and paired-end sequenced (41 cycles) using the NextSeq 500 system (Illumina).

Tumor B cells from indicated organs were sorted as CD19$^+$CD95$^+$GL7$^+$ (mice 1 and 4–6) or CD19$^+$CD95$^+$ (mice 2, 3, and 7) of sick Bhlhe40$^{-/-}$ mice (mice 1, 2, and 4–7) or a sick Rag2$^{-/-}$ recipient of Bhlhe40$^{-/-}$ lymphoma cells (mouse 3). Libraries were prepared as previously described (Kreslavsky et al., 2017) with minor modifications. In brief, RNA was isolated with RNeasy Plus Mini or Micro Kits (Qiagen; for mice 4 and 5, this step was performed after Trizol extraction), and mRNA was obtained by poly(A) selection with a Dynabeads mRNA purification kit (Thermo Fisher Scientific), followed by fragmentation by heating at 94°C for 3 min (in fragmentation buffer). The fragmented mRNA was used as a template for first-strand cDNA synthesis with random hexamers and a Superscript VILO cDNA Synthesis kit (Thermo Fisher Scientific). Second-strand cDNA was synthesized with 100 mM dATP, dCTP, dGTP, and dUTP in the presence of RNase H, Escherichia coli DNA polymerase I, and DNA ligase (Thermo Fisher Scientific). Sequencing libraries were prepared with the NEBNext Ultra II DNA Library Prep Kit for Illumina (NEB). For strand-specific RNA-seq, the uridines present in one cDNA strand were digested with uracil-N-glycosylase (NEB), as described (Parkhomchuk et al., 2009), followed by PCR amplification with NEBNext UltraII Q5 Master Mix (NEB). Libraries were subjected to Illumina deep sequencing (HiSeqV4 SR50 [mice 1 and 2] or NovaSeq SR100 [mice 3–7]). For RNA-seq analysis of polyclonal WT and Bhlhe40$^{-/-}$ GC B cells, LZ (CD19$^+$CD95$^+$GL7$^+$CXCR4^{lo}CD86^{hi}) and DZ (CD19$^+$CD95$^+$GL7$^+$CXCR4^{hi}CD86^{lo}) GC B cells were sorted from nonimmunized mixed BM chimeras and subjected to RNA-seq as discussed above for tumor cells. Tracks from DZ GC B cells are shown in Fig. 6 H.

Bioinformatic analysis of RNA-seq data

Sequence reads that passed the Illumina quality filtering were considered for alignment. Reads corresponding to mouse ribosomal RNAs (GenBank accession numbers BK000964.1 and NR046144.1) were removed. The remaining reads were cut down to a read length of 44 bp and aligned to the mouse transcriptome (genome assembly version of July 2007, NCBI37/mm9) using TopHat v1.4.1 (Trapnell et al., 2009) or RNA STAR (Dobin et al., 2013; Galaxy v2.7.8a; Afgan et al., 2018) for B cell and T cell RNA-seq datasets, respectively. The calculation of RNA expression values was all based on the RefSeq database, which was downloaded from University of California, Santa Cruz, on January 10, 2014. The annotation of Ig and T cell receptor genes was

incorporated from the Ensembl release 67 (Cunningham et al., 2015). Genes with overlapping exons were flagged, and double entries (i.e., exactly the same gene at two different genomic locations) were renamed. Genes with several transcripts were merged to consensus genes consisting of a union of all underlying exons using Fuge software (unpublished data), which resulted in 24,733 gene models.

For analysis of differential gene expression, the number of reads per gene was counted using HTseq v0.5.3 (Anders et al., 2015) with the overlap resolution mode set to union. The datasets were analyzed using the R package DESeq2 v1.2.10 (Love et al., 2014). Sample normalizations and dispersion estimations were conducted using the default DESeq2 settings. Transcripts per million were calculated from RNA-seq data, as described (Wagner et al., 2012).

GSEA was performed using the GSEA software from the Broad Institute (Subramanian et al., 2005). Genes were ranked on the basis of their change in expression (log_2 fold-change values) as determined by the DESeq2 package and were compared with gene sets from the MSigDB or defined gene sets from the literature or our data. GC B cell signature was used from Mabbott and Gray (2014) with *Bcl6* and *Gcsam* manually added to the signature. Early GC B cell signature was generated by pairwise comparison of our WT day 4 GC B and CCR6+ B cell datasets, using the top 500 GC B cell up-regulated genes.

scRNA-seq library preparation
For single-cell sequencing, WT and *Bhlhe40*−/− B1-8hi/+ B cells were cotransferred and sorted on day 3.5 (5 mice) and day 4 (5 mice) after immunization as described above for bulk RNA-seq. Cells from day 3.5 and 4 after immunization were pooled. An additional WT sample was sorted on day 2.5 after immunization. Lineage depletion for CD4/TCRβ/TCRγδ/CD11c/Gr1/NK1.1/Ter119/Igκ was performed using MACS anti-PE Micro-beads (Miltenyi Biotec). CD19+Igλ+CD45.1+CD45.2− (WT) and CD19+Igλ+CD45.1+CD45.2+ (*Bhlhe40*−/−) cells were double sorted using a FACS Aria III sorter. Broad gates were applied to include PBs that may start downregulating some of these surface molecules. For day 3.5–4 samples, cells were processed using the 10X Genomics kit v2 immediately after sorting. For day 2.5, cells were resuspended in cold PBS/0.04% BSA, fixed by adding 4 volumes of 100% Methanol (VWR), and incubated for 30 min at −20°C. Day 2.5 cells were stored at −80°C and also processed as described (Chen et al., 2018) using the 10X Genomics kit v3. Cells were sequenced paired end with 75-bp read length on a NextSeq550 system (Illumina).

Analysis of single-cell RNA-seq data
The sequenced 10X Chromium libraries from two samples were mapped to the mm10 mouse genome and assigned to droplets with Cell Ranger software (v3.0.1) with default parameters (Zheng et al., 2017). Transcriptomes of 7,324 WT cells with a median read coverage of 2,292 (day 2.5), 2,089 WT cells with a median read coverage of 2,507 (day 3.5–4), and 1,677 KO cells with a median read coverage of 3,823 (day 3.5–4) were obtained.

Joined embedding for days 2.5 and 3.5–4 was performed with Scanpy based on spliced transcripts from Velocyto (v0.17.13; La Manno et al., 2018). First, the data were normalized and filtered

with scanpy.pp.recipe_seurat workflow (Satija et al., 2015). Next, uniform manifold approximation and projection (UMAP) embedding was performed with default parameters. Cells were clustered with the Louvain algorithm (Blondel et al., 2008), and cell populations were defined as groups of clusters identified by this algorithm. GC B cell signature was used from Mabbott and Gray (2014) with *Bcl6* and *Gcsam* manually added to the signature. *BHLHE40* expression in the human tonsillar B cell scRNA-seq dataset was analyzed using Seurat object provided by the authors of the study (King et al., 2021; ArrayExpress accession no. E-MTAB-9005) with Seurat package v3 (Stuart et al., 2019).

Statistical analysis
Statistical analysis was performed with GraphPad Prism 8 software. Unpaired two-tailed Student's *t* test analysis was used to assess the statistical significance of one observed parameter between two experimental groups. Paired two-tailed Student's *t* test analysis was used to assess the statistical significance of one observed parameter between two related groups. The statistical evaluation of the RNA-seq data are described above.

Online supplemental material
Fig. S1 shows results further supporting the notion that Bhlhe40 restrains the GC reaction by a B cell–intrinsic mechanism. Fig. S2 contains data showing Bhlhe40 expression in activated B cells and documenting effects of Bhlhe40 deficiency early during the GC response. Results shown in Fig. S3 demonstrate that Bhlhe40 deficiency does not affect proliferation, apoptosis, or migration of activated B cells. Fig. S4 contains results of bulk RNA-seq, scRNA-seq, and ChIP-seq experiments aiming to characterize the molecular program downstream of Bhlhe40 in activated B cells. Fig. S5 shows a schematic diagram of the floxed *Bhlhe40* allele, contains results further describing the function of Bhlhe40 in T cells, and shows the expression of *Aicda* and *Igh* constant regions in Bhlhe40-deficient lymphoma cells.

Data availability
The RNA-seq, scRNA-seq, and ChIP-seq data generated for this study are available at the GEO repository under accession numbers GSE173673 and GSE186457.

References

Afgan, E., D. Baker, B. Batut, M. van den Beek, D. Bouvier, M. Čech, J. Chilton, D. Clements, N. Coraor, B.A. Grüning, et al. 2018. The Galaxy platform for accessible, reproducible and collaborative biomedical analyses: 2018 update. *Nucleic Acids Res.* 46(W1):W537–W544. https://doi.org/10.1093/nar/gky379

Anders, S., P.T. Pyl, and W. Huber. 2015. HTSeq--a Python framework to work with high-throughput sequencing data. *Bioinformatics.* 31:166–169. https://doi.org/10.1093/bioinformatics/btu638

Basso, K., and R. Dalla-Favera. 2015. Germinal centres and B cell lymphomagenesis. *Nat. Rev. Immunol.* 15:172–184. https://doi.org/10.1038/nri3814

Baumjohann, D., S. Preite, A. Reboldi, F. Ronchi, K.M. Ansel, A. Lanzavecchia, and F. Sallusto. 2013. Persistent antigen and germinal center B cells sustain T follicular helper cell responses and phenotype. *Immunity.* 38: 596–605. https://doi.org/10.1016/j.immuni.2012.11.020

Bertossi, A., M. Aichinger, P. Sansonetti, M. Lech, F. Neff, M. Pal, F.T. Wunderlich, H.-J. Anders, L. Klein, and M. Schmidt-Supprian. 2011. Loss of Roquin induces early death and immune deregulation but not autoimmunity. *J. Exp. Med.* 208:1749–1756. https://doi.org/10.1084/jem.20110578

Betz, B.C., K.L. Jordan-Williams, C. Wang, S.G. Kang, J. Liao, M.R. Logan, C.H. Kim, and E.J. Taparowsky. 2010. Batf coordinates multiple aspects of B and T cell function required for normal antibody responses. *J. Exp. Med.* 207:933–942. https://doi.org/10.1084/jem.20091548

Biram, A., and Z. Shulman. 2020. T cell help to B cells: Cognate and atypical interactions in peripheral and intestinal lymphoid tissues. *Immunol. Rev.* 296:36–47. https://doi.org/10.1111/imr.12890

Blondel, V.D., J.-L. Guillaume, R. Lambiotte, and E. Lefebvre. 2008. Fast unfolding of communities in large networks. *J. Stat. Mech.* 2008:P10008. https://doi.org/10.1088/1742-5468/2008/10/P10008

Bollig, N., A. Brüstle, K. Kellner, W. Ackermann, E. Abass, H. Raifer, B. Camara, C. Brendel, G. Giel, E. Bothur, et al. 2012. Transcription factor IRF4 determines germinal center formation through follicular T-helper cell differentiation. *Proc. Natl. Acad. Sci. USA.* 109:8664–8669. https://doi.org/10.1073/pnas.1205834109

Buenrostro, J.D., P.G. Giresi, L.C. Zaba, H.Y. Chang, and W.J. Greenleaf. 2013. Transposition of native chromatin for fast and sensitive epigenomic profiling of open chromatin, DNA-binding proteins and nucleosome position. *Nat. Methods.* 10:1213–1218. https://doi.org/10.1038/nmeth.2688

Calado, D.P., Y. Sasaki, S.A. Godinho, A. Pellerin, K. Köchert, B.P. Sleckman, I.M. de Alborán, M. Janz, S. Rodig, and K. Rajewsky. 2012. The cell-cycle regulator c-Myc is essential for the formation and maintenance of germinal centers. *Nat. Immunol.* 13:1092–1100. https://doi.org/10.1038/ni.2418

Cattoretti, G., L. Pasqualucci, G. Ballon, W. Tam, S.V. Nandula, Q. Shen, T. Mo, V.V. Murty, and R. Dalla-Favera. 2005. Deregulated BCL6 expression recapitulates the pathogenesis of human diffuse large B cell lymphomas in mice. *Cancer Cell.* 7:445–455. https://doi.org/10.1016/j.ccr.2005.03.037

Chen, J., F. Cheung, R. Shi, H. Zhou, and W. Lu. CHI Consortium. 2018. PBMC fixation and processing for Chromium single-cell RNA sequencing. *J. Transl. Med.* 16:198. https://doi.org/10.1186/s12967-018-1578-4

Cheng, C.L., and S. O'Connor. 2017. T cell-rich lymphoid infiltrates with large B cells: a review of key entities and diagnostic approach. *J. Clin. Pathol.* 70:187–201. https://doi.org/10.1136/jclinpath-2016-204065

Chou, C., D.J. Verbaro, E. Tonc, M. Holmgren, M. Cella, M. Colonna, D. Bhattacharya, and T. Egawa. 2016. The Transcription Factor AP4 Mediates Resolution of Chronic Viral Infection through Amplification of Germinal Center B Cell Responses. *Immunity.* 45:570–582. https://doi.org/10.1016/j.immuni.2016.07.023

Crotty, S. 2019. T Follicular Helper Cell Biology: A Decade of Discovery and Diseases. *Immunity.* 50:1132–1148. https://doi.org/10.1016/j.immuni.2019.04.011

Cunningham, F., M.R. Amode, D. Barrell, K. Beal, K. Billis, S. Brent, D. Carvalho-Silva, P. Clapham, G. Coates, S. Fitzgerald, et al. 2015. Ensembl 2015. *Nucleic Acids Res.* 43(Database issue, D1):D662–D669. https://doi.org/10.1093/nar/gku1010

de Boer, J., A. Williams, G. Skavdis, N. Harker, M. Coles, M. Tolaini, T. Norton, K. Williams, K. Roderick, A.J. Potocnik, and D. Kioussis. 2003. Transgenic mice with hematopoietic and lymphoid specific expression of Cre. *Eur. J. Immunol.* 33:314–325. https://doi.org/10.1002/immu.200310005

De Silva, N.S., and U. Klein. 2015. Dynamics of B cells in germinal centres. *Nat. Rev. Immunol.* 15:137–148. https://doi.org/10.1038/nri3804

de Vinuesa, C.G., M.C. Cook, J. Ball, M. Drew, Y. Sunners, M. Cascalho, M. Wabl, G.G.B. Klaus, and I.C.M. MacLennan. 2000. Germinal centers without T cells. *J. Exp. Med.* 191:485–494. https://doi.org/10.1084/jem.191.3.485

Dent, A.L., A.L. Shaffer, X. Yu, D. Allman, and L.M. Staudt. 1997. Control of inflammation, cytokine expression, and germinal center formation by BCL-6. *Science.* 276:589–592. https://doi.org/10.1126/science.276.5312.589

Dobin, A., C.A. Davis, F. Schlesinger, J. Drenkow, C. Zaleski, S. Jha, P. Batut, M. Chaisson, and T.R. Gingeras. 2013. STAR: ultrafast universal RNA-seq aligner. *Bioinformatics.* 29:15–21. https://doi.org/10.1093/bioinformatics/bts635

Dominguez-Sola, D., G.D. Victora, C.Y. Ying, R.T. Phan, M. Saito, M.C. Nussenzweig, and R. Dalla-Favera. 2012. The proto-oncogene MYC is required for selection in the germinal center and cyclic reentry. *Nat. Immunol.* 13:1083–1091. https://doi.org/10.1038/ni.2428

Dominguez-Sola, D., J. Kung, A.B. Holmes, V.A. Wells, T. Mo, K. Basso, and R. Dalla-Favera. 2015. The FOXO1 Transcription Factor Instructs the Germinal Center Dark Zone Program. *Immunity.* 43:1064–1074. https://doi.org/10.1016/j.immuni.2015.10.015

Feng, J., T. Liu, B. Qin, Y. Zhang, and X.S. Liu. 2012. Identifying ChIP-seq enrichment using MACS. *Nat. Protoc.* 7:1728–1740. https://doi.org/10.1038/nprot.2012.101

Finkin, S., H. Hartweger, T.Y. Oliveira, E.E. Kara, and M.C. Nussenzweig. 2019. Protein Amounts of the MYC Transcription Factor Determine Germinal Center B Cell Division Capacity. *Immunity.* 51:324–336.e5. https://doi.org/10.1016/j.immuni.2019.06.013

Fukuda, T., T. Yoshida, S. Okada, M. Hatano, T. Miki, K. Ishibashi, S. Okabe, H. Koseki, S. Hirosawa, M. Taniguchi, et al. 1997. Disruption of the Bcl6 gene results in an impaired germinal center formation. *J. Exp. Med.* 186: 439–448. https://doi.org/10.1084/jem.186.3.439

Gertz, J., K.E. Varley, N.S. Davis, B.J. Baas, I.Y. Goryshin, R. Vaidyanathan, S. Kuersten, and R.M. Myers. 2012. Transposase mediated construction of RNA-seq libraries. *Genome Res.* 22:134–141. https://doi.org/10.1101/gr.127373.111

Glaros, V., R. Rauschmeier, A.V. Artemov, A. Reinhardt, S. Ols, A. Emmanouilidi, C. Gustafsson, Y. You, C. Mirabello, Å.K. Björklund, et al. 2021.

Limited access to antigen drives generation of early B cell memory while restraining the plasmablast response. *Immunity.* 54:2005–2023.e10. https://doi.org/10.1016/j.immuni.2021.08.017

Gustafsson, C., A. De Paepe, C. Schmidl, and R. Mansson. 2018. High-Throughput ChIPmentation: freely scalable, single day ChIPseq data generation from very low cell-numbers. *bioRxiv* (Preprint posted September 27, 2018)https://doi.org/10.1101/426957

Hatzi, K., J.P. Nance, M.A. Kroenke, M. Bothwell, E.K. Haddad, A. Melnick, and S. Crotty. 2015. BCL6 orchestrates Tfh cell differentiation via multiple distinct mechanisms. *J. Exp. Med.* 212:539–553. https://doi.org/10.1084/jem.20141380

Hobeika, E., S. Thiemann, B. Storch, H. Jumaa, P.J. Nielsen, R. Pelanda, and M. Reth. 2006. Testing gene function early in the B cell lineage in mb1-cre mice. *Proc. Natl. Acad. Sci. USA.* 103:13789–13794. https://doi.org/10.1073/pnas.0605944103

Huynh, J.P., C.-C. Lin, J.M. Kimmey, N.N. Jarjour, E.A. Schwarzkopf, T.R. Bradstreet, I. Shchukina, O. Shpynov, C.T. Weaver, R. Taneja, et al. 2018. Bhlhe40 is an essential repressor of IL-10 during *Mycobacterium tuberculosis* infection. *J. Exp. Med.* 215:1823–1838. https://doi.org/10.1084/jem.20171704

Inoue, T., R. Shinnakasu, W. Ise, C. Kawai, T. Egawa, and T. Kurosaki. 2017. The transcription factor Foxo1 controls germinal center B cell proliferation in response to T cell help. *J. Exp. Med.* 214:1181–1198. https://doi.org/10.1084/jem.20161263

Ise, W., M. Kohyama, B.U. Schraml, T. Zhang, B. Schwer, U. Basu, F.W. Alt, J. Tang, E.M. Oltz, T.L. Murphy, and K.M. Murphy. 2011. The transcription factor BATF controls the global regulators of class-switch recombination in both B cells and T cells. *Nat. Immunol.* 12:536–543. https://doi.org/10.1038/ni.2037

Ise, W., K. Fujii, K. Shiroguchi, A. Ito, K. Kometani, K. Takeda, E. Kawakami, K. Yamashita, K. Suzuki, T. Okada, and T. Kurosaki. 2018. T Follicular Helper Cell-Germinal Center B Cell Interaction Strength Regulates Entry into Plasma Cell or Recycling Germinal Center Cell Fate. *Immunity.* 48:702–715.e4. https://doi.org/10.1016/j.immuni.2018.03.027

Johnston, R.J., A.C. Poholek, D. DiToro, I. Yusuf, D. Eto, B. Barnett, A.L. Dent, J. Craft, and S. Crotty. 2009. Bcl6 and Blimp-1 are reciprocal and antagonistic regulators of T follicular helper cell differentiation. *Science.* 325:1006–1010. https://doi.org/10.1126/science.1175870

Kanda, M., H. Yamanaka, S. Kojo, Y. Usui, H. Honda, Y. Sotomaru, M. Harada, M. Taniguchi, N. Suzuki, T. Atsumi, et al. 2016. Transcriptional regulator Bhlhe40 works as a cofactor of T-bet in the regulation of IFN-γ production in iNKT cells. *Proc. Natl. Acad. Sci. USA.* 113:E3394–E3402. https://doi.org/10.1073/pnas.1604178113

King, H.W., N. Orban, J.C. Riches, A.J. Clear, G. Warnes, S.A. Teichmann, and L.K. James. 2021. Single-cell analysis of human B cell maturation predicts how antibody class switching shapes selection dynamics. *Sci. Immunol.* 6:eabe6291. https://doi.org/10.1126/sciimmunol.abe6291

Kreslavsky, T., B. Vilagos, H. Tagoh, D.K. Poliakova, T.A. Schwickert, M. Wöhner, M. Jaritz, S. Weiss, R. Taneja, M.J. Rossner, and M. Busslinger. 2017. Essential role for the transcription factor Bhlhe41 in regulating the development, self-renewal and BCR repertoire of B-1a cells. *Nat. Immunol.* 18:442–455. https://doi.org/10.1038/ni.3694

Kwon, K., C. Hutter, Q. Sun, I. Bilic, C. Cobaleda, S. Malin, and M. Busslinger. 2008. Instructive role of the transcription factor E2A in early B lymphopoiesis and germinal center B cell development. *Immunity.* 28:751–762. https://doi.org/10.1016/j.immuni.2008.04.014

La Manno, G., R. Soldatov, A. Zeisel, E. Braun, H. Hochgerner, V. Petukhov, K. Lidschreiber, M.E. Kastriti, P. Lönnerberg, A. Furlan, et al. 2018. RNA velocity of single cells. *Nature.* 560:494–498. https://doi.org/10.1038/s41586-018-0414-6

Langmead, B., and S.L. Salzberg. 2012. Fast gapped-read alignment with Bowtie 2. *Nat. Methods.* 9:357–359. https://doi.org/10.1038/nmeth.1923

Lee, P.P., D.R. Fitzpatrick, C. Beard, H.K. Jessup, S. Lehar, K.W. Makar, M. Pérez-Melgosa, M.T. Sweetser, M.S. Schlissel, S. Nguyen, et al. 2001. A critical role for Dnmt1 and DNA methylation in T cell development, function, and survival. *Immunity.* 15:763–774. https://doi.org/10.1016/S1074-7613(01)00227-8

Li, C., B. Zhu, Y.M. Son, Z. Wang, L. Jiang, M. Xiang, Z. Ye, K.E. Beckermann, Y. Wu, J.W. Jenkins, et al. 2019. The Transcription Factor Bhlhe40 Programs Mitochondrial Regulation of Resident CD8^{+} T Cell Fitness and Functionality. *Immunity.* 51:491–507.e7. https://doi.org/10.1016/j.immuni.2019.08.013

Lin, C.-C., T.R. Bradstreet, E.A. Schwarzkopf, J. Sim, J.A. Carrero, C. Chou, L.E. Cook, T. Egawa, R. Taneja, T.L. Murphy, et al. 2014. Bhlhe40 controls cytokine production by T cells and is essential for pathogenicity in

autoimmune neuroinflammation. *Nat. Commun.* 5:3551. https://doi.org/10.1038/ncomms4551

Love, M.I., W. Huber, and S. Anders. 2014. Moderated estimation of fold change and dispersion for RNA-seq data with DESeq2. *Genome Biol.* 15:550. https://doi.org/10.1186/s13059-014-0550-8

Mabbott, N.A., and D. Gray. 2014. Identification of co-expressed gene signatures in mouse B1, marginal zone and B2 B-cell populations. *Immunology.* 141:79–95. https://doi.org/10.1111/imm.12171

Machanick, P., and T.L. Bailey. 2011. MEME-ChIP: motif analysis of large DNA datasets. *Bioinformatics.* 27:1696–1697. https://doi.org/10.1093/bioinformatics/btr189

Mesin, L., J. Ersching, and G.D. Victora. 2016. Germinal Center B Cell Dynamics. *Immunity.* 45:471–482. https://doi.org/10.1016/j.immuni.2016.09.001

Miyazaki, K., M. Miyazaki, Y. Guo, N. Yamasaki, M. Kanno, Z. Honda, H. Oda, H. Kawamoto, and H. Honda. 2010. The role of the basic helix-loop-helix transcription factor Dec1 in the regulatory T cells. *J. Immunol.* 185:7330–7339. https://doi.org/10.4049/jimmunol.1001381

Nurieva, R.I., Y. Chung, G.J. Martinez, X.O. Yang, S. Tanaka, T.D. Matskevitch, Y.-H. Wang, and C. Dong. 2009. Bcl6 mediates the development of T follicular helper cells. *Science.* 325:1001–1005. https://doi.org/10.1126/science.1176676

Ochiai, K., M. Maienschein-Cline, G. Simonetti, J. Chen, R. Rosenthal, R. Brink, A.S. Chong, U. Klein, A.R. Dinner, H. Singh, and R. Sciammas. 2013. Transcriptional regulation of germinal center B and plasma cell fates by dynamical control of IRF4. *Immunity.* 38:918–929. https://doi.org/10.1016/j.immuni.2013.04.009

Oestreich, K.J., S.E. Mohn, and A.S. Weinmann. 2012. Molecular mechanisms that control the expression and activity of Bcl-6 in TH1 cells to regulate flexibility with a TFH-like gene profile. *Nat. Immunol.* 13:405–411. https://doi.org/10.1038/ni.2242

Okazaki, I.M., H. Hiai, N. Kakazu, S. Yamada, M. Muramatsu, K. Kinoshita, and T. Honjo. 2003. Constitutive expression of AID leads to tumorigenesis. *J. Exp. Med.* 197:1173–1181. https://doi.org/10.1084/jem.20030275

Ow, J.R., Y.H. Tan, Y. Jin, A.G. Bahirvani, and R. Taneja. 2014. Stra13 and Sharp-1, the Non-Grouchy Regulators of Development and Disease. *In* Current Topics in Developmental Biology. T. Reshma, editor. Academic Press, Cambridge, MA; 317–338.

Parkhomchuk, D., T. Borodina, V. Amstislavskiy, M. Banaru, L. Hallen, S. Krobitsch, H. Lehrach, and A. Soldatov. 2009. Transcriptome analysis by strand-specific sequencing of complementary DNA. *Nucleic Acids Res.* 37:e123. https://doi.org/10.1093/nar/gkp596

Pasqualucci, L., G. Bhagat, M. Jankovic, M. Compagno, P. Smith, M. Muramatsu, T. Honjo, H.C. Morse III, M.C. Nussenzweig, and R. Dalla-Favera. 2008. AID is required for germinal center-derived lymphomagenesis. *Nat. Genet.* 40:108–112. https://doi.org/10.1038/ng.2007.35

Picelli, S., O.R. Faridani, Å.K. Björklund, G. Winberg, S. Sagasser, and R. Sandberg. 2014. Full-length RNA-seq from single cells using Smart-seq2. *Nat. Protoc.* 9:171–181. https://doi.org/10.1038/nprot.2014.006

Revilla-i-Domingo, R., I. Bilic, B. Vilagos, H. Tagoh, A. Ebert, I.M. Tamir, L. Smeenk, J. Trupke, A. Sommer, M. Jaritz, and M. Busslinger. 2012. The B-cell identity factor Pax5 regulates distinct transcriptional programmes in early and late B lymphopoiesis. *EMBO J.* 31:3130–3146. https://doi.org/10.1038/emboj.2012.155

Robinson, M.J., Z. Ding, C. Pitt, E.J. Brodie, I. Quast, D.M. Tarlinton, and D. Zotos. 2020. The amount of BCL6 in B cells shortly after antigen engagement determines their representation in subsequent germinal centers. *Cell Rep.* 30:1530–1541.e4. https://doi.org/10.1016/j.celrep.2020.01.009

Rossner, M.J., H. Oster, S.P. Wichert, L. Reinecke, M.C. Wehr, J. Reinecke, G. Eichele, R. Taneja, and K.-A. Nave. 2008. Disturbed clockwork resetting in Sharp-1 and Sharp-2 single and double mutant mice. *PLoS One.* 3:e2762. https://doi.org/10.1371/journal.pone.0002762

Sander, S., V.T. Chu, T. Yasuda, A. Franklin, R. Graf, D.P. Calado, S. Li, K. Imami, M. Selbach, M. Di Virgilio, et al. 2015. PI3 Kinase and FOXO1 Transcription Factor Activity Differentially Control B Cells in the Germinal Center Light and Dark Zones. *Immunity.* 43:1075–1086. https://doi.org/10.1016/j.immuni.2015.10.021

Satija, R., J.A. Farrell, D. Gennert, A.F. Schier, and A. Regev. 2015. Spatial reconstruction of single-cell gene expression data. *Nat. Biotechnol.* 33:495–502. https://doi.org/10.1038/nbt.3192

Schwickert, T.A., G.D. Victora, D.R. Fooksman, A.O. Kamphorst, M.R. Mugnier, A.D. Gitlin, M.L. Dustin, and M.C. Nussenzweig. 2011. A dynamic T

cell-limited checkpoint regulates affinity-dependent B cell entry into the germinal center. *J. Exp. Med.* 208:1243–1252. https://doi.org/10.1084/jem.20102477

Scott, D.W., and R.D. Gascoyne. 2014. The tumour microenvironment in B cell lymphomas. *Nat. Rev. Cancer.* 14:517–534. https://doi.org/10.1038/nrc3774

Seimiya, M., A. Wada, K. Kawamura, A. Sakamoto, Y. Ohkubo, S. Okada, M. Hatano, T. Tokuhisa, T. Watanabe, H. Saisho, et al. 2004. Impaired lymphocyte development and function in Clast5/Stra13/DEC1-transgenic mice. *Eur. J. Immunol.* 34:1322–1332. https://doi.org/10.1002/eji.200324700

Shaffer, A.L., X. Yu, Y. He, J. Boldrick, E.P. Chan, and L.M. Staudt. 2000. BCL-6 represses genes that function in lymphocyte differentiation, inflammation, and cell cycle control. *Immunity.* 13:199–212. https://doi.org/10.1016/S1074-7613(00)00020-0

Shih, T.-A.Y., M. Roederer, and M.C. Nussenzweig. 2002. Role of antigen receptor affinity in T cell-independent antibody responses in vivo. *Nat. Immunol.* 3:399–406. https://doi.org/10.1038/ni776

Shinkai, Y., G. Rathbun, K.-P. Lam, E.M. Oltz, V. Stewart, M. Mendelsohn, J. Charron, M. Datta, F. Young, A.M. Stall, and F.W. Alt. 1992. RAG-2-deficient mice lack mature lymphocytes owing to inability to initiate V(D)J rearrangement. *Cell.* 68:855–867. https://doi.org/10.1016/0092-8674(92)90029-C

Srinivas, S., T. Watanabe, C.S. Lin, C.M. William, Y. Tanabe, T.M. Jessell, and F. Costantini. 2001. Cre reporter strains produced by targeted insertion of EYFP and ECFP into the ROSA26 locus. *BMC Dev. Biol.* 1:4. https://doi.org/10.1186/1471-213X-1-4

Stone, E.L., M. Pepper, C.D. Katayama, Y.M. Kerdiles, C.-Y. Lai, E. Emslie, Y.C. Lin, E. Yang, A.W. Goldrath, M.O. Li, et al. 2015. ICOS coreceptor signaling inactivates the transcription factor FOXO1 to promote Tfh cell differentiation. *Immunity.* 42:239–251. https://doi.org/10.1016/j.immuni.2015.01.017

Stuart, T., A. Butler, P. Hoffman, C. Hafemeister, E. Papalexi, W.M. Mauck III, Y. Hao, M. Stoeckius, P. Smibert, and R. Satija. 2019. Comprehensive Integration of Single-Cell Data. *Cell.* 177:1888–1902.e21. https://doi.org/10.1016/j.cell.2019.05.031

Suan, D., N.J. Kräutler, J.L.V. Maag, D. Butt, K. Bourne, J.R. Hermes, D.T. Avery, C. Young, A. Statham, M. Elliott, et al. 2017. CCR6 Defines Memory B Cell Precursors in Mouse and Human Germinal Centers, Revealing Light-Zone Location and Predominant Low Antigen Affinity. *Immunity.* 47:1142–1153.e4. https://doi.org/10.1016/j.immuni.2017.11.022

Subramanian, A., P. Tamayo, V.K. Mootha, S. Mukherjee, B.L. Ebert, M.A. Gillette, A. Paulovich, S.L. Pomeroy, T.R. Golub, E.S. Lander, and J.P. Mesirov. 2005. Gene set enrichment analysis: a knowledge-based approach for interpreting genome-wide expression profiles. *Proc. Natl. Acad. Sci. USA.* 102:15545–15550. https://doi.org/10.1073/pnas.0506580102

Sun, H., B. Lu, R.Q. Li, R.A. Flavell, and R. Taneja. 2001. Defective T cell activation and autoimmune disorder in Stra13-deficient mice. *Nat. Immunol.* 2:1040–1047. https://doi.org/10.1038/ni721

Taylor, J.J., M.K. Jenkins, and K.A. Pape. 2012a. Heterogeneity in the differentiation and function of memory B cells. *Trends Immunol.* 33:590–597. https://doi.org/10.1016/j.it.2012.07.005

Taylor, J.J., K.A. Pape, and M.K. Jenkins. 2012b. A germinal center-independent pathway generates unswitched memory B cells early in the primary response. *J. Exp. Med.* 209:597–606. https://doi.org/10.1084/jem.20111696

Trapnell, C., L. Pachter, and S.L. Salzberg. 2009. TopHat: discovering splice junctions with RNA-Seq. *Bioinformatics.* 25:1105–1111. https://doi.org/10.1093/bioinformatics/btp120

Turner, C.A. Jr., D.H. Mack, and M.M. Davis. 1994. Blimp-1, a novel zinc finger-containing protein that can drive the maturation of B lymphocytes into immunoglobulin-secreting cells. *Cell.* 77:297–306. https://doi.org/10.1016/0092-8674(94)90321-2

Vinuesa, C.G., M.C. Cook, C. Angelucci, V. Athanasopoulos, L. Rui, K.M. Hill, D. Yu, H. Domaschenz, B. Whittle, T. Lambe, et al. 2005. A RING-type ubiquitin ligase family member required to repress follicular helper T cells and autoimmunity. *Nature.* 435:452–458. https://doi.org/10.1038/nature03555

Wagner, G.P., K. Kin, and V.J. Lynch. 2012. Measurement of mRNA abundance using RNA-seq data: RPKM measure is inconsistent among samples. *Theory Biosci.* 131:281–285. https://doi.org/10.1007/s12064-012-0162-3

Willis, S.N., K.L. Good-Jacobson, J. Curtis, A. Light, J. Tellier, W. Shi, G.K. Smyth, D.M. Tarlinton, G.T. Belz, L.M. Corcoran, et al. 2014. Transcription factor IRF4 regulates germinal center cell formation through a B cell-intrinsic mechanism. *J. Immunol.* 192:3200–3206. https://doi.org/10.4049/jimmunol.1303216

Yang, H., H. Wang, C.S. Shivalila, A.W. Cheng, L. Shi, and R. Jaenisch. 2013. One-step generation of mice carrying reporter and conditional alleles by CRISPR/Cas-mediated genome engineering. *Cell.* 154:1370–1379. https://doi.org/10.1016/j.cell.2013.08.022

Ye, B.H., G. Cattoretti, Q. Shen, J. Zhang, N. Hawe, R. de Waard, C. Leung, M. Nouri-Shirazi, A. Orazi, R.S.K. Chaganti, et al. 1997. The BCL-6 proto-oncogene controls germinal-centre formation and Th2-type inflammation. *Nat. Genet.* 16:161–170. https://doi.org/10.1038/ng0697-161

Yoshida, H., C.A. Lareau, R.N. Ramirez, S.A. Rose, B. Maier, A. Wroblewska, F. Desland, A. Chudnovskiy, A. Mortha, C. Dominguez, et al. Immunological Genome Project. 2019. The cis-Regulatory Atlas of the Mouse Immune System. *Cell.* 176:897–912.e20. https://doi.org/10.1016/j.cell.2018.12.036

Yu, D., S. Rao, L.M. Tsai, S.K. Lee, Y. He, E.L. Sutcliffe, M. Srivastava, M. Linterman, L. Zheng, N. Simpson, et al. 2009. The transcriptional repressor Bcl-6 directs T follicular helper cell lineage commitment. *Immunity.* 31:457–468. https://doi.org/10.1016/j.immuni.2009.07.002

Yu, F., S. Sharma, D. Jankovic, R.K. Gurram, P. Su, G. Hu, R. Li, S. Rieder, K. Zhao, B. Sun, and J. Zhu. 2018. The transcription factor Bhlhe40 is a switch of inflammatory versus antiinflammatory Th1 cell fate determination. *J. Exp. Med.* 215:1813–1821. https://doi.org/10.1084/jem.20170155

Zheng, G.X.Y., J.M. Terry, P. Belgrader, P. Ryvkin, Z.W. Bent, R. Wilson, S.B. Ziraldo, T.D. Wheeler, G.P. McDermott, J. Zhu, et al. 2017. Massively parallel digital transcriptional profiling of single cells. *Nat. Commun.* 8:14049. https://doi.org/10.1038/ncomms14049
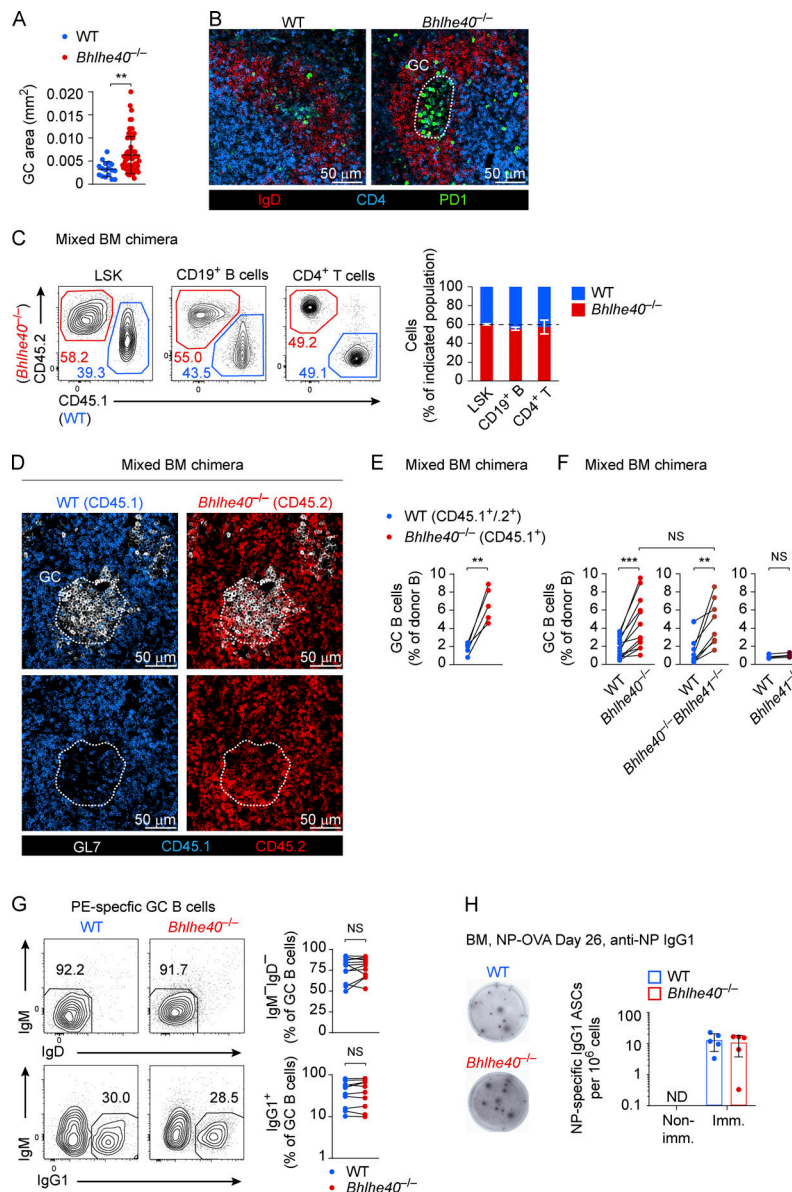
Supplemental material

Figure S1. **Bhlhe40 restrains the GC reaction by a B cell–intrinsic mechanism. (A and B)** Spleen sections of unchallenged WT and *Bhlhe40⁻/⁻* mice as analyzed by confocal immunofluorescence microscopy. **(A)** The area of spontaneous GCs was determined by measuring the size of IgD-negative areas within B cell follicles. Pooled data obtained with two mice for each genotype are shown. **(B)** Spontaneous GCs, identified by PD1 (green) expression in IgD (red)-negative areas, are highlighted. One experiment is shown. **(C–F)** Mixed BM chimeras were generated by transferring a 1:1 (C and F) or 4:1 (D) mixture of WT (CD45.1⁺) and *Bhlhe40⁻/⁻* (CD45.2⁺; C and D) or *Bhlhe40⁻/⁻Bhlhe41⁻/⁻* (CD45.2⁺) or *Bhlhe41⁻/⁻* (CD45.2⁺; F) BM progenitor cells into lethally irradiated *Rag2⁻/⁻* recipients. Mice were analyzed >6 wk after transfer. **(C)** Flow cytometric analysis and quantification of WT and *Bhlhe40⁻/⁻* donor-derived cells among BM Lin⁻Sca-1⁺Kit⁺ (LSK) cells, CD19⁺ B cells, and CD4⁺ T cells is shown. One experiment with four mice, representative of four independent experiments performed, is shown. **(D)** Representative images of spleen sections of 4:1 WT and *Bhlhe40⁻/⁻* mixed BM chimera. Spontaneous GCs, identified by GL7 (white) expression, are highlighted. WT donor-derived CD45.1⁺ cells are shown in blue, and *Bhlhe40⁻/⁻* donor-derived CD45.2⁺ cells in red. Note depletion of WT cells from the GC area. **(E)** Mixed BM chimeras were generated by transferring a 1:1 ratio of WT (CD45.1⁺/CD45.2⁺) and *Bhlhe40⁻/⁻* (CD45.1⁺) BM progenitor cells into lethally irradiated WT (CD45.2⁺) recipients. Quantification of flow cytometric analysis of GC B cells among WT and *Bhlhe40⁻/⁻* CD19⁺ B cells is shown. One experiment with five mice, representative of two independent experiments, is shown. **(F)** Quantification of flow cytometric analysis of GC B cells in mixed BM chimeras among WT and *Bhlhe40⁻/⁻*, *Bhlhe40⁻/⁻Bhlhe41⁻/⁻*, and *Bhlhe41⁻/⁻* CD19⁺ B cells is shown. Pooled data from two independent experiments with n = 12 (WT and *Bhlhe40⁻/⁻*), n = 8 (*Bhlhe40⁻/⁻Bhlhe41⁻/⁻*), and n = 4 (*Bhlhe41⁻/⁻*) mice are shown. **(G)** Frequency of IgM⁻IgD⁻ (top) and IgG1⁺ (bottom) Ig class-switched cells among total PE-specific GC B cells from PE-immunized mixed WT; *Bhlhe40⁻/⁻* BM chimeras were determined 21 d after immunization (based on the experiment shown in Fig. 1 E). **(H)** Antibody secretion by WT and *Bhlhe40⁻/⁻* BM plasma cells 26 d after immunization (imm.) with NP-OVA (in alum). The numbers of NP-specific IgG1 ASCs were determined by ELISPOT assay by incubating BM cells on NP₂₅-BSA–coated plates before determination of the ELISPOT numbers as described in Materials and methods. Images of representative ELISPOT wells (left) and the mean cell numbers with SD (right) are shown. Non-imm., nonimmunized. ND, not detectable. One experiment with n = 5 NP-OVA–immunized mice and n = 3 nonimmunized mice for each genotype is shown. Representative of two independent experiments. One dot represents one mouse. Data were analyzed with unpaired two-tailed Student's *t* test (A, mean ± SD is shown), paired two-tailed Student's *t* test (E, G), or two-tailed Wilcoxon matched-pairs signed-rank test (F). **, P < 0.01; ***, P < 0.001. One dot represents one analyzed GC (A) or one mouse (E–H).
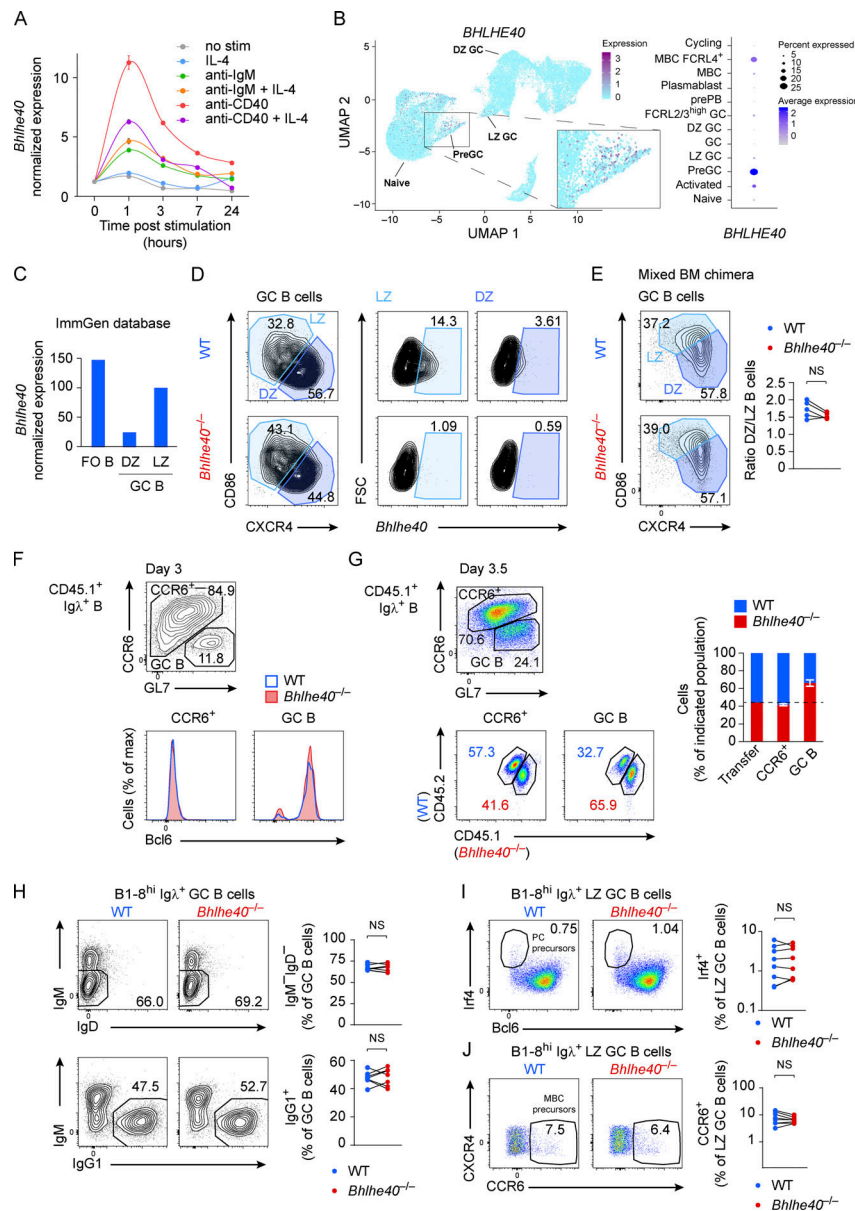
Figure S2. **Bhlhe40 expression in activated B cells and effects of Bhlhe40 deficiency early during the GC response. (A)** *Bhlhe40* expression in in vitro activated B cells is shown. Naive CD43⁻ B cells from the spleens of WT mice were cultured for ≤1 d in the presence of either anti-IgM or anti-CD40 antibody alone or in combination with IL-4. *Bhlhe40* expression (normalized to *Hprt*) was measured by qRT-PCR. Each data point represents the mean value with SEM of three technical replicates. Data are representative of two independent experiments. **(B)** UMAP and dot plot showing expression of *BHLHE40* by human tonsillar B cells as revealed by scRNA-seq. Population annotation as in the original publication (King et al., 2021). **(C)** *Bhlhe40* expression in follicular (FO) B and LZ and DZ GC B cells. RNA-seq data from the ImmGen database are shown. **(D)** *Bhlhe40* expression in LZ and DZ GC B cells as assessed by RNA flow cytometry. Data are representative of two independent experiments. FSC, forward scatter. **(E)** Mixed BM chimeras were generated by transferring a 1:1 mixture of WT (CD45.1⁺) and *Bhlhe40⁻/⁻* (CD45.2⁺) BM progenitor cells into lethally irradiated *Rag2⁻/⁻* recipients. Mice were analyzed >6 wk after transfer. Flow cytometric analysis and quantification of the DZ/LZ ratio of WT and *Bhlhe40⁻/⁻* GC B cells are shown. One experiment with five mice is shown and is representative of three independent experiments. Data were analyzed with paired two-tailed Student's *t* test; NS, P > 0.05. One dot represents one mouse. **(F–J)** OVA-primed CD45.2⁺ WT mice were injected with a 1:1 mixture of WT (CD45.1⁺) and *Bhlhe40⁻/⁻* (CD45.1⁺/CD45.2⁺; F and H) or WT (CD45.1⁺/CD45.2⁺) and *Bhlhe40⁻/⁻* (CD45.1⁺; G, I, and J) B1-8ʰⁱ splenocytes and immunized with NP-OVA in alum the next day. See schematic representation in Fig. 2 A. **(F)** Surface expression of CCR6 and GL7 on CD45.1⁺Igλ⁺CD19⁺ B cells on day 3 after immunization. Intracellular expression of Bcl6 in WT and *Bhlhe40⁻/⁻* CCR6⁺ and GC B cells is shown. Representative staining for 1 of 10 mice is shown. The results are representative of four independent experiments. **(G)** Surface expression of CCR6 and GL7 on CD45.1⁺Igλ⁺CD19⁺ B cells on day 3.5 after immunization. Representative flow cytometric analysis and quantification of WT and *Bhlhe40⁻/⁻* donor-derived cells among CCR6⁺ and GC B cells are shown. One experiment with 11 mice is shown and is representative of at least three independent experiments. **(H)** Frequency of IgM⁻IgD⁻ (top) and IgG1⁺ (bottom) Ig class-switched cells among B1-8ʰⁱ WT and *Bhlhe40⁻/⁻* donor-derived Igλ⁺ GC B cells on day 7 after NP-OVA immunization. Results are representative of two independent experiments. **(I)** Frequency of Irf4⁺Bcl6ˡᵒ PC precursors among B1-8ʰⁱ WT and *Bhlhe40⁻/⁻* donor-derived Igλ⁺ LZ (CD86ʰⁱCXCR4ˡᵒ) GC B cells on day 9–10 after immunization. Results of a single experiment harvested on two consecutive days. **(J)** Frequency of CCR6⁺ MBC precursors among B1-8ʰⁱ WT and *Bhlhe40⁻/⁻* donor-derived Igλ⁺ LZ (CD86ʰⁱCXCR4ˡᵒ) GC B cells on day 9 after immunization. Results pooled from two independent experiments.
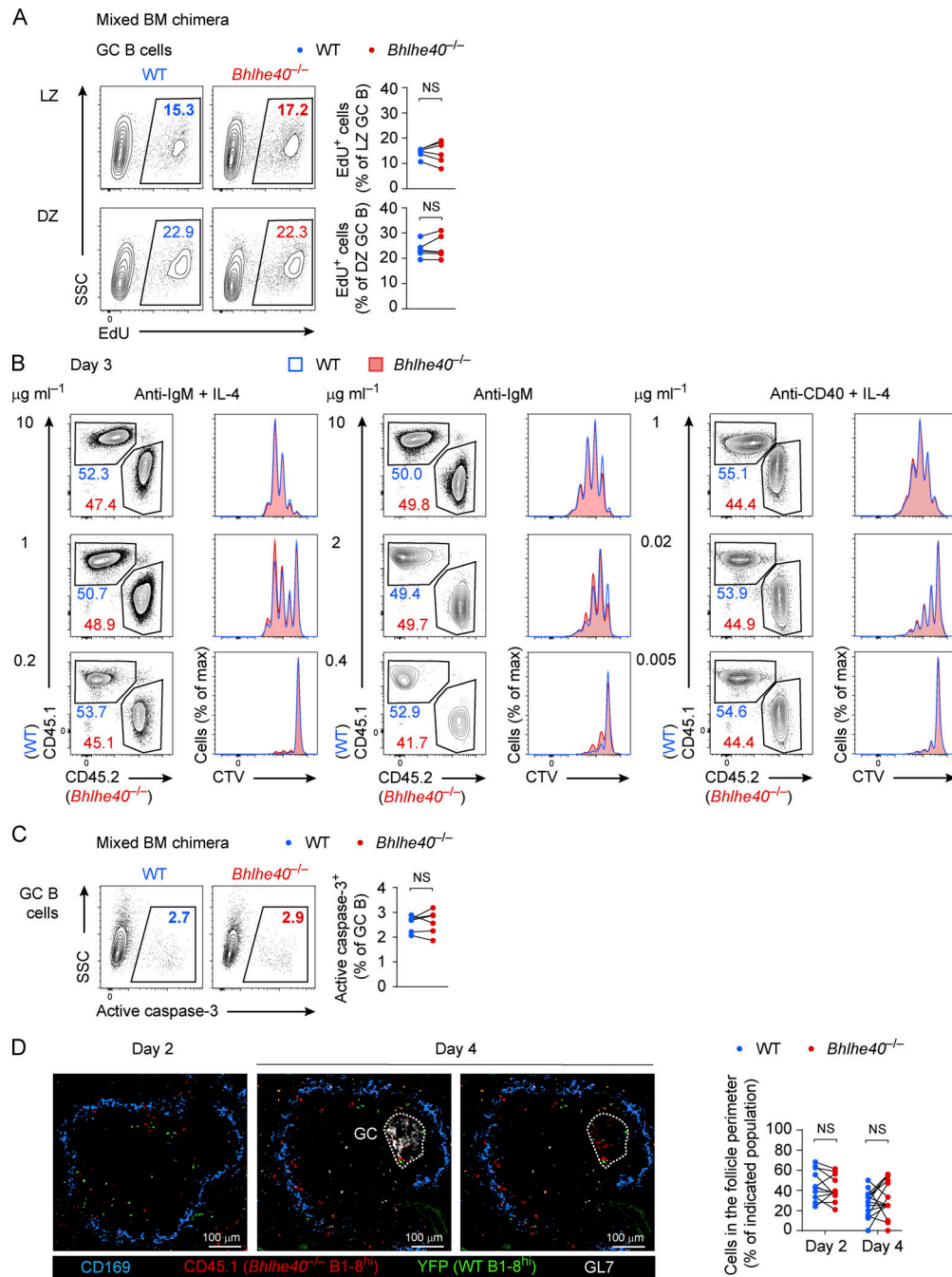
Figure S3. **Bhlhe40 deficiency does not affect proliferation, apoptosis, or migration of activated B cells. (A and C)** Mixed BM chimeras were generated by transferring a 1:1 mixture of WT (CD45.1[+]) and *Bhlhe40*^{−/−} (CD45.2[+]) BM progenitor cells into lethally irradiated *Rag2*^{−/−} recipients. Flow cytometric analysis and quantification assessing the proliferation of LZ and DZ WT and *Bhlhe40*^{−/−} GC B cells (A) as well as determining the frequency of apoptotic cells in WT and *Bhlhe40*^{−/−} GC B cells (C). EdU was i.v. injected 2 h before analysis (A), and apoptotic cells were identified by intracellular staining for active caspase-3 (C). Pooled data from two independent experiments with six mice are shown. Data were analyzed with paired two-tailed Student's *t* test; NS, P > 0.05. One dot represents one mouse. SSC, side scatter. **(B)** Naive CD43^{−} B cells from the spleens of WT (CD45.1^{+}) and *Bhlhe40*^{−/−} (CD45.2^{+}) mice were mixed in a 1:1 ratio and labeled with CellTrace Violet (CTV) dye. Cells were kept in culture for 3 d in the presence of decreasing concentrations of either anti-CD40 or anti-IgM antibody alone or in combination with 20 ng/ml of IL-4. The ratio of WT and *Bhlhe40*^{−/−} cells among live cells on day 3 of culture and the CTV dilution are depicted. Representative data of one experiment with *n* = 3 mice are shown and are representative of two independent experiments. **(D)** OVA-primed CD45.2[+] WT mice were injected with a 1:1 mixture of sorted Igκ[−]lin[−] WT (*Cd23*-Cre *Rosa26*-LSL-YFP) and *Bhlhe40*^{−/−} (CD45.1[+]) B1-8[hi] splenocytes and were immunized with NP-OVA in alum the next day. Representative images of spleen sections on days 2 and 4 after immunization are shown (left). GCs, identified by GL7 (white) expression, are highlighted. WT donor-derived YFP^{+} cells are shown in green, and *Bhlhe40*^{−/−} donor-derived CD45.1^{+} cells in red. Individual color channels were adjusted. Note the similar distribution of WT and *Bhlhe40*^{−/−} cells in the perimeter (as identified by CD169 expression) and within the B cell follicle, as well as the depletion of WT cells from the GC area on day 4 after immunization. Quantification of the frequency of cells located in the follicle perimeter was determined as described in Materials and methods. One experiment with *n* = 2 mice per time point is shown and is representative of two independent experiments. One dot represents one counted image.
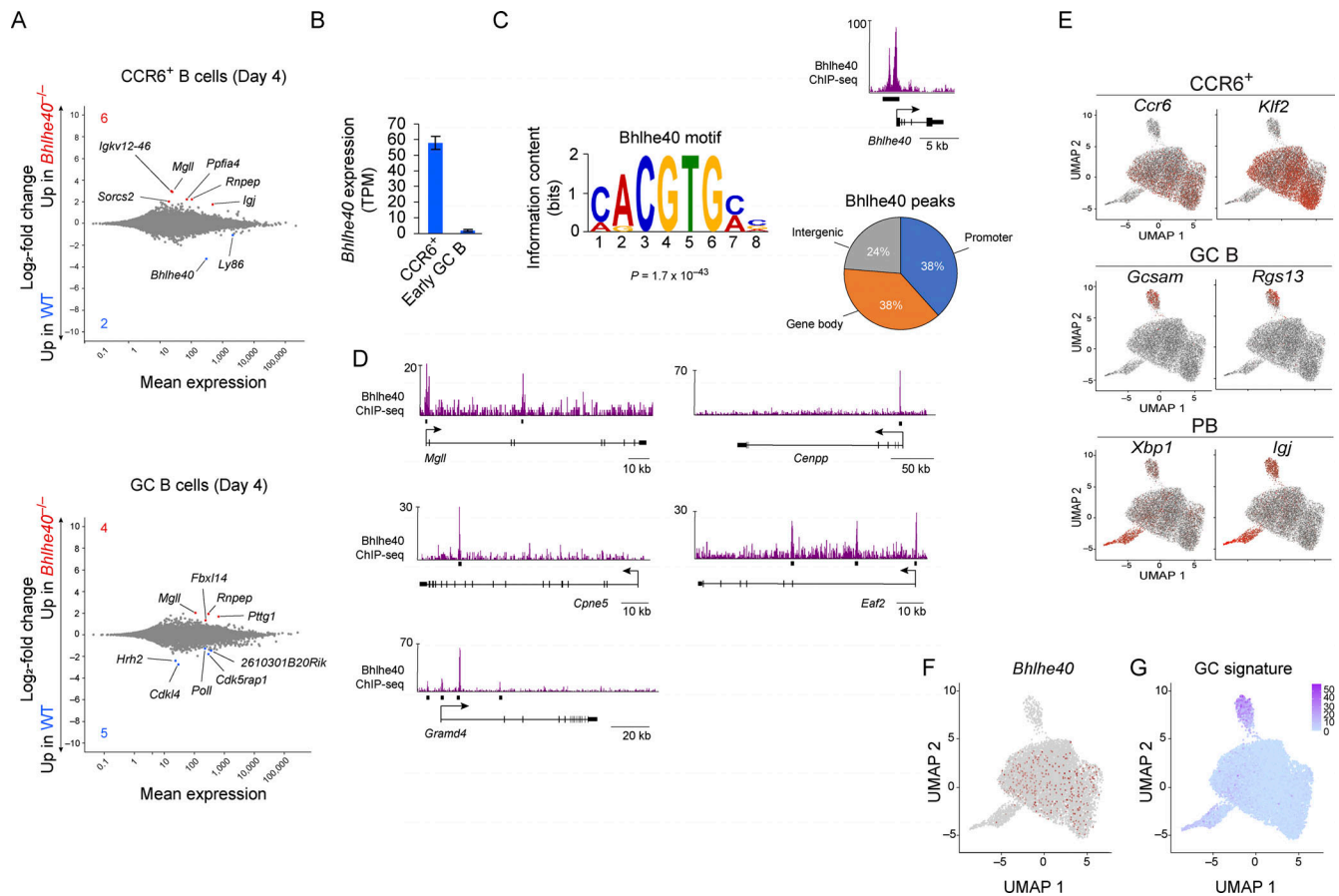
Rauschmeier et al.
Bhlhe40 in the germinal center reaction

Journal of Experimental Medicine   S4
https://doi.org/10.1084/jem.20211406

Figure S4. **Comparison of gene expression changes in WT and _Bhlhe40_$^{-/-}$ CCR6$^+$ and early GC B cells. (A and B)** OVA-primed CD45.2$^+$ WT mice were injected with a 1:1 mixture of WT (CD45.1$^+$) and _Bhlhe40_$^{-/-}$ (CD45.1$^+$/CD45.2$^+$) B1-8^{hi} splenocytes and immunized with NP-OVA in alum the next day. RNA-seq analysis of double-sorted WT and _Bhlhe40_$^{-/-}$ CCR6$^+$ and early GC B cells was performed on day 4 after immunization. **(A)** Comparison of changes in gene expression induced by Bhlhe40 deficiency in WT CCR6$^+$ cells (top) and WT early GC B cells (bottom). Log$_2$-transformed _Bhlhe40_$^{-/-}$/WT fold-changes are plotted. All significantly changed (twofold or more, adjusted P < 0.1) genes are highlighted, and the number of such up- and down-regulated genes is indicated. **(B)** _Bhlhe40_ expression in CCR6$^+$ and early GC B cells. TPM, transcripts per million. **(C)** ChIP-seq analysis of Bhlhe40 binding in in vitro activated B cells. Naive CD43$^-$ B cells from the spleen were activated in the presence of anti-CD40 for 4 h. Left: The consensus Bhlhe40-binding motif was identified by the de novo motif-discovery program MEME-ChIP. Right top: Example of Bhlhe40 binding at the _Bhlhe40_ gene. Right bottom: Distribution of Bhlhe40 peaks at intergenic regions, gene bodies, or promoters. **(D)** Bhlhe40 binding at the indicated gene loci (expression of the corresponding genes is shown in Fig. 3 C). Bars below the tracks represent called peaks. **(E–G)** scRNA-seq analysis of B cell activation as in Fig. 3 D. UMAP plots highlight the expression of CCR6$^+$ B cell–, GC B cell–, and PB-enriched genes (E), _Bhlhe40_ (F), and the GC B cell signature genes (G). Only WT cells in the scRNA-seq dataset are shown in F.
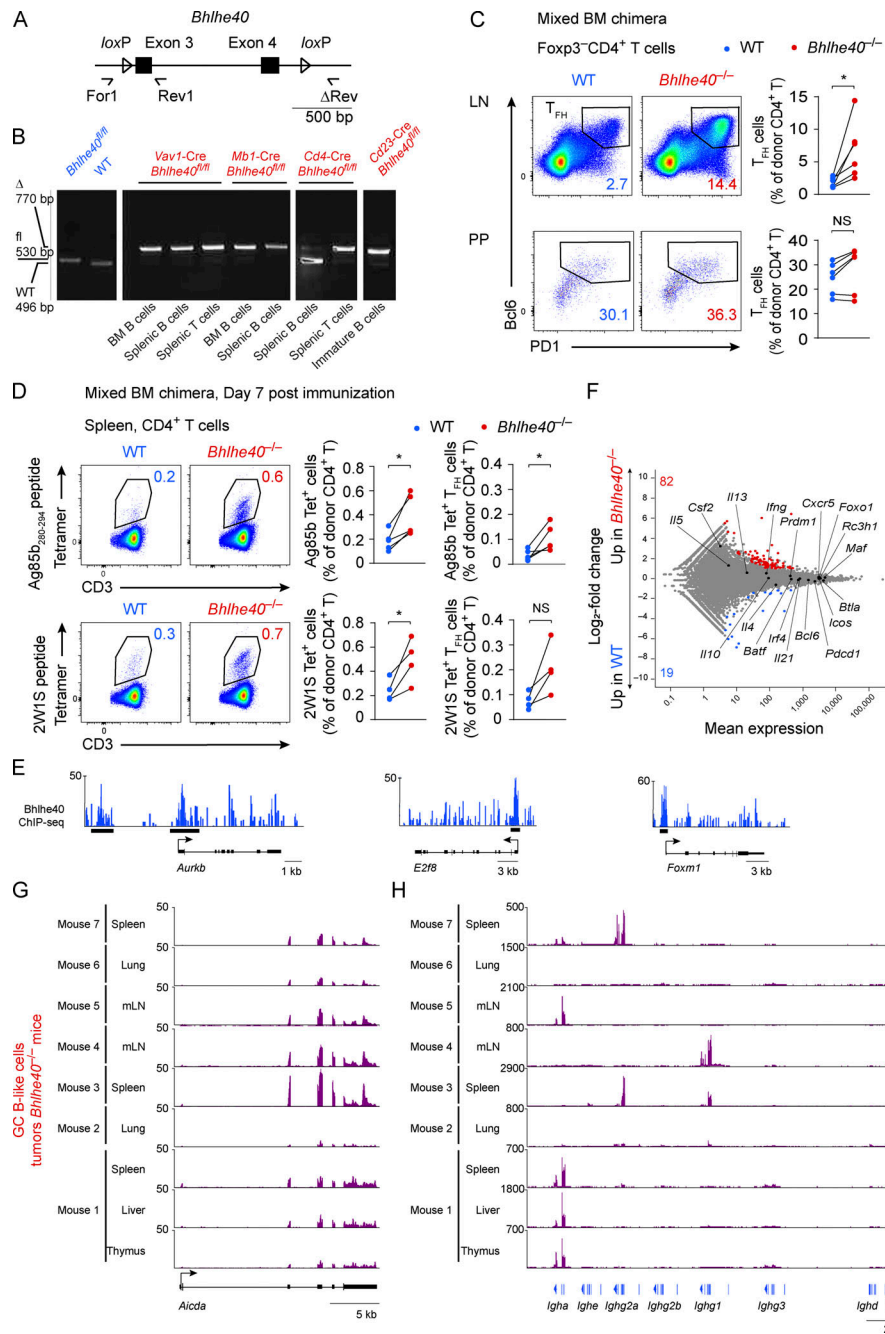
Figure S5. **Deletion efficiencies of the *lox*P-flanked *Bhlhe40* allele; Bhlhe40 restrains T$_{FH}$ cell numbers. (A)** Schematic representation of the floxed *Bhlhe40* allele. **(B)** Deletion efficiency of the *Bhlhe40* allele in *Vav1*-Cre *Bhlhe40*$^{fl/fl}$, *Mb1*-Cre *Bhlhe40*$^{fl/fl}$, *Cd4*-Cre *Bhlhe40*$^{fl/fl}$, and *Cd23*-Cre *Bhlhe40*$^{fl/fl}$ mice as determined by PCR with the primers indicated in A. **(C)** Mixed BM chimeras were generated by transferring a 1:1 mixture of WT (CD45.1$^+$) and *Bhlhe40*$^{-/-}$ (CD45.2$^+$) BM progenitor cells into lethally irradiated *Rag2*$^{-/-}$ recipients. Mice were analyzed >6 wk after transfer. Expression of PD1 and Bcl6 by WT and *Bhlhe40*$^{-/-}$ Foxp3$^-$CD4$^+$ T cells and quantification of T$_{FH}$ cells among WT and *Bhlhe40*$^{-/-}$ Foxp3$^-$CD4$^+$ T cells from the LNs and Peyer's patches (PP) is shown. One experiment with six mice is shown and is representative of two independent experiments. **(D and F)** Mixed BM chimeras were generated by transferring a 1:1 mixture of WT (CD45.1$^+$/CD45.2$^+$) and *Bhlhe40*$^{-/-}$ (CD45.1$^+$) BM progenitor cells into lethally irradiated WT (CD45.2$^+$) recipients. Mice were immunized with the *M. tuberculosis* Ag85b$_{280-294}$ (D and F) or 2W1S (F) peptide emulsified in complete Freund's adjuvant >7 wk after transfer. **(D)** Flow cytometric analysis and quantification of Ag85b- and 2W1S-tetramer–binding CD4$^+$ T cells and T$_{FH}$ cells among WT and *Bhlhe40*$^{-/-}$ CD4$^+$ T cells in the spleen on day 7 after immunization. For each condition, one experiment with four mice is shown and is representative of one to two independent experiments. Data were analyzed with paired two-tailed Student's *t* test; NS, P > 0.05; *, P < 0.05. One dot represents one mouse. **(E)** ChIP-seq analysis of Bhlhe40 binding at the indicated cell cycle–related gene loci in in vitro activated CD4$^+$ T cells (data from a published dataset; Huynh et al., 2018). **(F)** Comparison of changes in gene expression induced by Bhlhe40 deficiency in Ag85b-tetramer–binding CD4$^+$ T cells, as shown by RNA-seq analysis of Ag85b-tetramer–binding WT and *Bhlhe40*$^{-/-}$ CD4$^+$ T cells isolated from mixed BM chimeras 11 d after immunization. Log$_2$-transformed *Bhlhe40*$^{-/-}$/WT fold-changes are plotted, and the number of significantly (twofold or more, adjusted P < 0.1) up- and down-regulated genes is indicated. T$_{FH}$ cell–related genes and selected cytokine-encoding genes are highlighted. Note that the expression of none of these genes was significantly changed. **(G and H)** RNA-seq analysis of *Bhlhe40*$^{-/-}$ GC B-like lymphoma cells. The mRNA expression profile of lymphoma cells at the *Aicda* (G) and *Igh* (H) loci are shown as in Fig. 6 H. mLN, mesenteric lymph node.

Rauschmeier et al.
Bhlhe40 in the germinal center reaction

Journal of Experimental Medicine   S6
https://doi.org/10.1084/jem.20211406